Advances in Colloid and Interface Science 256 (2018) 48–64

Contents lists available at ScienceDirect

Advances in Colloid and Interface Science

journal homepage: www.elsevier.com/locate/cis

Historical perspective

An overview of the transport of liquid molecules through structured polymer films, barriers and composites – Experiments correlated to structure-based simulations

Sofie Gårdebjer [a,b], Mikael Larsson [b,c,d], Tobias Gebäck [b,f], Marie Skepö [a,b], Anette Larsson [b,e,*]

[a] Lund University, P.O. Box 124, 221 00 Lund, Sweden
[b] SuMo BIOMATERIALS, Chalmers University of Technology, 412 96 Gothenburg, Sweden
[c] School of Energy and Resources, University College London, 220 Victoria Square, Adelaide, SA, 5000, Australia
[d] Future Industries Institute, University of South Australia, Mawson Lakes Campus, SA 5095, Australia
[e] Chalmers University of Technology, 412 96 Gothenburg, Sweden
[f] Department of Mathematical Sciences, Chalmers University of Technology and Gothenburg University, 412 96 Gothenburg, Sweden

ARTICLE INFO

Available online 25 May 2018

ABSTRACT

Films engineered to control the transport of liquids are widely used through society. Examples include barriers in packaging, wound care products, and controlled release coatings in pharmaceutics. When observed at the macroscopic scale such films commonly appear homogeneous, however, a closer look reveals a complex nano- and microstructure that together with the chemical properties of the different domains control the transport properties. In this review we compare and discuss macroscopic transport properties, measured using the straightforward, yet highly powerful technique "modified Ussing chambers", also denoted side-by-side diffusion cells, for a wide range of structured polymer films and composites. We also discuss and compare the macroscopic observations and conclusions on materials properties with that of lattice Boltzmann simulations of transport properties based on underlying material structure and chemistry. The survey of the field: (i) highlights the use and power of modified Ussing Chambers for determining liquid transport properties of polymer films, (ii) demonstrates the predictability in both directions between macroscopic observations of transport using modified Ussing chambers and structure-based simulations, and (iii) provides experimental and theoretical insights regarding the transport-determining properties of structured polymer films and composites.

© 2018 Elsevier B.V. All rights reserved.

Contents

* Corresponding author at: SuMo BIOMATERIALS, Chalmers University of Technology, 412 96 Gothenburg, Sweden.
E-mail address: anette.larsson@chalmers.se (A. Larsson).

https://doi.org/10.1016/j.cis.2018.05.004
0001-8686/© 2018 Elsevier B.V. All rights reserved.

1. Introduction

People use different types of barriers in their daily life, for examples in packaging, wound care products, and pharmaceutical coatings [1–4]. Many barriers today are based on polymers due to reduced costs, fast production etc. [5]. Polymeric barriers can be produced via a wide range of methods including extrusion, spray coating, casting, moulding etc., where the choice of technique depends on the final application. Different approaches will also result in different types of material structures: the reader is refereed to Fig. 1 for an overview of examples of structures discussed in this review. Combinations of different polymers are often essential to obtain all desired characteristics of the final application.

Non-porous/dense films and laminates are examples of common structures in different types of packaging. In these cases the properties of the polymers are combined, and one layer may serve as an oxygen barrier, while another layer may function as a moisture barrier, whereas the third layer provides the consumer with information about the content [2,6]. A composite is a material that consists of a polymer matrix and a filler. These materials can also be used as packaging materials [7]. Here, the filler is commonly included to enhance the mechanical properties of the material and the particles are generally considered to be impermeable. Thus, an addition of filler should in theory result in improved barrier properties [8,9]. However, in reality, incompatibility between the filler and the matrix due to the differences in the surface chemistry may result in voids in the material and an increased permeability as a consequence [10–12].

Materials with controlled transport properties can also be formed by combining polymers with limited miscibility. For example, by a suitable combination of water-soluble and water-insoluble polymers, a film can be formed where the components have phase-separated into distinct regions [13]. Upon exposure to water the soluble component will leak out, leaving a porous skeleton of the water-insoluble polymer [14–17]. Porous films are commonly used as pharmaceutical coatings, and the pores can be either connected or disconnected depending on the desired release profile, where the connected pores are expected to result in a faster release of a pharmaceutical active ingredient. By varying the composition and/or the preparation conditions, the transport properties of such films can be controlled with great precision [15,18,19]. A complicating factor in predicting the transport through coatings/films in complex environments is that polymers are prone to swell in compatible solvents and that the diffusion in polymer matrixes is strongly dependent on the volume fraction of polymer [20]. An increase in the diffusion coefficient with decreasing volume fraction of polymer may also be counteracted by the swelling, causing blockage of pores, and an increased diffusion distance due to macroscopic volume increase. For example, this has been shown to be of relevance to the performance of pharmaceutical controlled release coatings in presence of alcohol [21] since there is a risk of dose dumping [22]. The latter might result in a peak in the plasma of the drug, which can have fatal consequences for the patient.

Factors known to affect the rate of transport through a membrane are, for example, crystallinity, type and concentration of fillers, compatibilizers and/or plasticizers, as well as the chemical structure of the polymer (molecular weight, degree of cross-linking, taciticity etc.). In general, two types of models are used to explain the permeability and the mass transport mechanisms in polymer materials: (i) models based on the motion of polymer chains and the permeant in combination with intermolecular forces, and (ii) models with a foundation in free volume theory, considering the relationship between the diffusion coefficient and the free volume present in the polymer [23]. Extensive reviews of these models can be found elsewhere [20,24].

The most important property for barrier materials is however to withstand the transport of liquids and gases in both and/or one direction, for example to protect a product from the environment, and thereby avoid degradation/contamination. Even though the films may seem homogenous from a macroscopic point of view, it may differ significantly on the micro- and nanoscopic level. To be able to design materials with desired properties it is crucial to understand the structure-transport correlations, which can be performed either by measuring or simulating the permeability. For this purpose, it is of importance to study both the gas permeability and the transport of solvent molecules or molecules dissolved in solvent (liquid permeability). Several reviews on gas transport are available in the literature [25–28]. Liquid permeability can be advantageously measured by utilizing modified Ussing chambers, which is an experimental setup for measuring the diffusion of permeants through a barrier material. The original chambers were invented by a Danish zoologist and physiologist named Hans Henriksen Ussing and the main idea is to measure the vectorial ion transport through epithelial skin [29]. The chambers have also been used to measure the transport of ions, nutrients, and drugs across epithelial tissues in vitro [30,31]. Side-by-side diffusion cells are also commonly used and resemble modified Ussing chambers. The latter can be used for many different purposes related to diffusion, and the focus of this review will be on studies where molecules, such as water, different pharmaceutical drugs, and juice ingredients, have been used to measure transport over different types of barriers.

The aim of this review is to present the applicability of using modified Ussing chambers and side-by-side diffusion cells to correlate diffusion through complex materials to their structures on nano- and

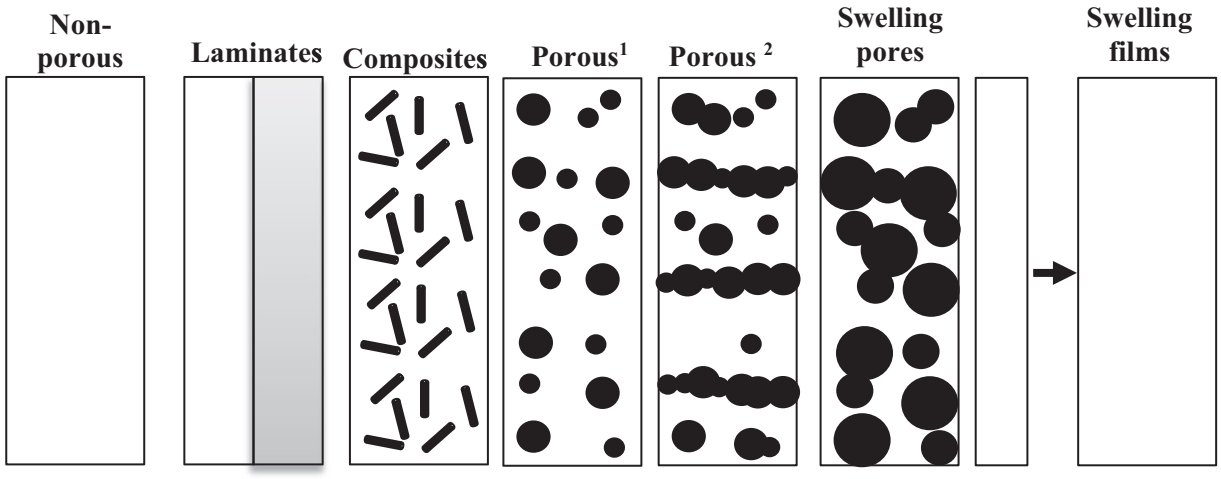

Fig. 1. Schematic drawings of different film structures discussed in this review, (1) corresponds to disconnected and (2) to connected pores.

microscale. In addition, a short introduction to how computer simulations on a microstructure level may contribute to a more detailed picture about the diffusion transport mechanism through a material is provided.

2. Basic concepts of permeability of polymeric materials

2.1. Theoretical and mathematical models for calculation of permeability

Small molecules can often dissolve and diffuse in polymer materials. Quite intuitively, the rate of transport of molecules across a film depends on the solubility of the molecules in the film and their diffusive movement [32,33]. Thomas Graham recognized this already in year 1866 and formulated the Solution-Diffusion model [34]. It has been much effort devoted to both the solution and diffusion step under different scenarios, as summarized in literature [20,32,33]. However, from a macroscopic and simplistic perspective, the following key steps are present: (i) the permeant dissolves in the film, (ii) there is a net diffusion of the permeant along the chemical potential gradient and, (iii) the permeant leaves the film by dissolving in the external solution (schematically shown in Fig. 2).

The extent to which a permeant dissolves in the film in step (i) is commonly described by the partition coefficient (K), which is the ratio between the concentration of permeant in the solution and the film at equilibrium. The partition coefficient is a critical parameter as it describes the concentration of permeant in the film surface and thus the number of molecules available to diffuse through the film. The diffusive motion of permeant molecules in step (ii) derives from random molecular motion of individual molecules. The rate of this motion depends on the size and the chemistry of the molecule, the structure and the chemistry of the matrix where the diffusion occur (which is affected by absorption of the solvent), the temperature, the pressure, and the viscosity [20]. It is important to remember that there will always be molecules diffusing in both directions across a film, but the driving force for a net diffusive transport in one direction is often well approximated by the chemical potential gradient over the film, which under ideal conditions is the concentration gradient divided by the concentration times a factor RT (where R is the gas constant and T is the temperature).

Once a permeant molecule has passed the film, the extent to which the molecules leave the film in step (iii) depends on the solubility of the permeant in the film and in the receiving solution. This can be easily visualized that if zero-concentration of the permeant is maintained in the solution, and if any molecule that leaves the film is immediately removed through mixing, the solubility of the permeant in the solution would have little effect. However, this is not the case in reality. In proximity to the outer boundary of the film, there will be a stagnant layer also denoted the diffusive layer, whose thickness decreases with increased mixing of the solution. Molecules in this layer will, as in the film, diffuse randomly in all directions, and can thereby leave the stagnant layer either by re-entering the film or disappearing into the bulk solution. If the solubility of the permeant is high (low chemical potential) in this layer than the film, the permeant molecules will readily leave the film and enter the solution. However, if the solubility is higher in the film than in the solution, the molecules will be less prone to leave the film and fewer molecules will diffuse across the stagnant layer over a given time. Based on steps (i)-(iii), the transport of molecules across a film is fundamentally dependent on the diffusion and the solubility of the permeant molecules. When characterizing the permeability of films, well-defined experimental setups are commonly employed based on the below theory.

The most common way to *macroscopically* describe the diffusion through a film is by Fick's law:

$$J = -Ac\frac{D}{RT}\frac{\partial \mu}{\partial z}, \tag{1}$$

where J is the mass transfer rate (mol/s), A is the cross-sectional area of the film, D is the diffusion coefficient, μ is chemical potential, and z is distance in the direction of the film thickness. For an ideal system, the chemical potential is $\mu = \mu_0 + RT \ln c$, where c is the concentration, and thus:

$$J = -AD\frac{\partial c}{\partial z}. \tag{2}$$

For an ideal system involving diffusion over a *homogenous film* with constant value of D, the following expression is valid at pseudo-steady state, i.e., when the concentration of the permeant within the film does not vary with time (see Fig. 2a):

$$J = \frac{DA}{h}(c_1 - c_2), \tag{3}$$

where h is the thickness of the film, c_1 and c_2 are the concentrations in the donor and acceptor surface of the film, respectively (see Fig. 2),

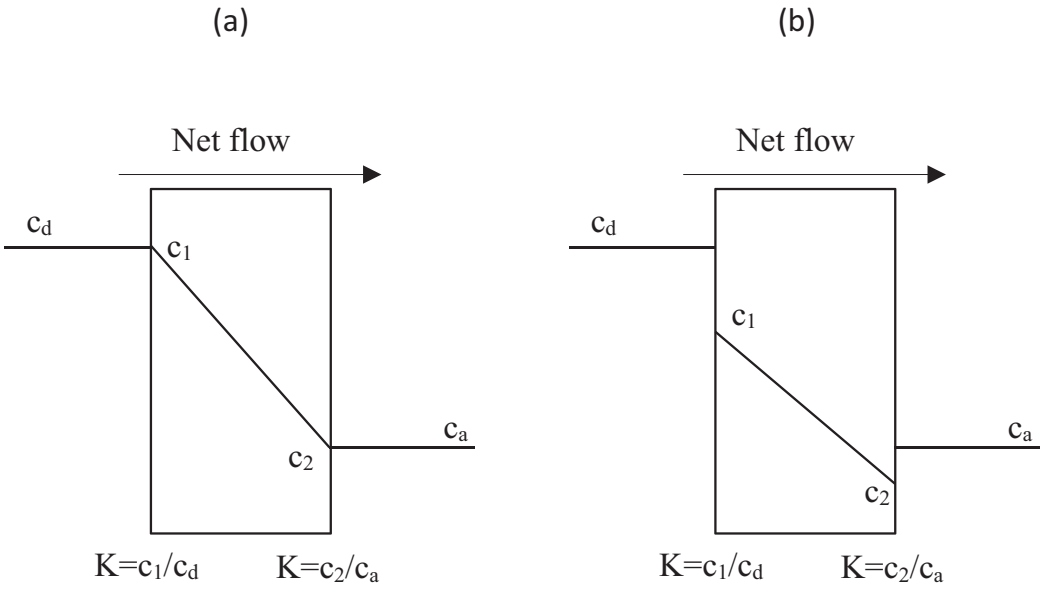

Fig. 2. Schematic image of the linear concentration decline reached at steady state when the partition coefficient (a) K > 1 and (b) K < 1.

and c_1 and c_2 can be related to the concentrations in the donor and acceptor chamber by incorporation of the partition coefficient. If the same solvent is used in both chambers, and if it is assumed that stagnant layers are negligible, then the partition coefficient relates to the concentrations in the film and in the chambers as:

$$K = \frac{c_1}{c_d} = \frac{c_2}{c_a}, \tag{4}$$

where c_d and c_a are the concentrations in the donor and acceptor chamber, respectively. Eqs. (3) and (4) can be combined to:

$$J = DKA\frac{(c_d - c_a)}{h} = PA\frac{(c_d - c_a)}{h} \tag{5}$$

where $P = DK$ is commonly referred to as the permeability. Here the authors would like to emphasize that in some literature the permeability is defined as $P = DKh^{-1}$. This notation refers to the mass transport across a film with a specific thickness, rather than the fundamental, geometry-independent, mass-transport properties in a film material. Due to its simplicity, Eq. (5) is commonly used to evaluate the permeability or barrier properties of films using macroscopic measurements, such as discussed in Section 2.2.

For a *porous film*, where the concentration and the diffusion of the permeant in the film material can be neglected in comparison to the solvent-filled pores, the corresponding expression can be derived. However, in this case, P is equivalent to an effective diffusion coefficient D_e:

$$D_e = \frac{D_p \varepsilon F(\lambda)}{\tau^2} \tag{6}$$

where D_p is the diffusion coefficient of the permeant free in solution [35–37] or in the pores of the film [38]. The latter should be better adapted for films where the pores present an environment significantly different from the bulk solution, for example, gel-filled volumes. The porosity ε, the hindrance factor $F(\lambda)$, and the tortuosity τ, represent pore structure-related parameters and are discussed in more detail by Larsson et al. [39]. Note that since it is assumed that the chemical environment in the pores is equivalent to that in the solvent, the partition coefficient is not present in the equation.

Based on Eqs. (2)–(5), van den Mooter and co-workers developed a useful expression to determine the permeability of the samples [40]. Under the assumptions that: (i) a linear concentration profile within the film has been reached, (ii) that the aqueous boundary layers on both sides of the film do not affect the total transport process, and (iii) equal volumes (V) of the donor and acceptor chamber, the following equation was derived:

$$\frac{2PA}{hV}t = -\ln\left(\frac{c_{d,0} - 2c_a(t)}{c_{d,0}}\right), \tag{7}$$

where the latter assumes that $c_a = 0$ when $t = 0$. From Eq. (7), the permeability can be obtained from the slope obtained by $-\ln(c_{d,0}\text{-}2c_a/c_{d,0})$ versus time. Thus, by knowing the initial concentration in the donor chamber ($c_{d,0}$), and monitoring the concentration in the acceptor chamber, the permeability is straight-forward to determine. For more details on the different models presented here, several reviews, articles, and books are available [20,32,33,35–38,40].

2.2. Modified Ussing chambers and side-by-side diffusion cells for measurement of the permeability

Liquid permeability (or diffusion) through films can be measured by utilizing diffusion cells, for example modified Ussing chambers, as shown schematically in Fig. 3a. These cells consist of a donor and acceptor chamber, between which the film to be studied is positioned. The chambers are filled with liquid (usually water), and the permeant of interest is added to the donor chamber. The transport of the permeant across the film is subsequently elucidated by monitoring the increase of the concentration in the acceptor chamber. When extracting samples from the acceptor chamber for analysis, it is critical to immediately replenish the extracted volume with fresh solution to minimize the impact of film pressure gradients. Graphs similar to Fig. 3b are usually acquired for the permeant concentration in the acceptor chamber as a function of time, and by applying for example Eqs. (4) or (5), the permeability, and/or the diffusion coefficient can be calculated.

Permeability can also be measured by using side-by-side diffusion cells. These cells are very similar to the modified Ussing chambers except that stirring is often achieved by a magnetic stirrer in the donor and/or acceptor chamber, instead of applying a rotating table or stirrers. Both types of setups can either be directly coupled to a detection source, such a UV-VIS spectrophotometer or by sampling manually [42,43].

By determining the concentration of the permeant in the two different chambers in the diffusion cell, it should be possible to quantify the permeant, preferably by using straightforward and readily accessible methods and equipment. An alternative, as already mentioned, is by UV/VIS-detection. The former requires that the molecule absorbs light in the measurable range, which is often the case for conjugated compounds. Additionally, radioactive labelled permeants are attractive

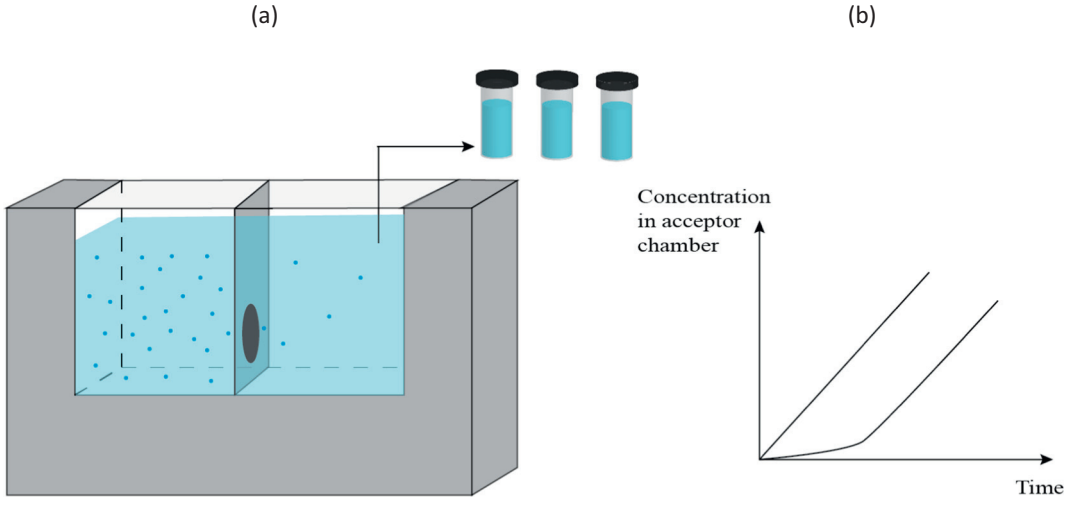

Fig. 3. Schematic image of (a) a modified Ussing chamber, and (b) example of typical graphs of the concentration of the permeant in the acceptor chamber as a function of time [41].

as their excellent detectability enables the usage of very low concentrations, allowing for small osmotic pressure differences between the chambers. Osmotic pressure differences can be further eliminated by adding the corresponding non-labelled molecule to the acceptor chamber. This will, ideally, result in the equal chemical potential in the donor and in the acceptor chamber, and labelled and non-labelled molecules will simultaneously diffuse through the film, whereas only the labelled ones will be detected. This approach is particularly useful in evaluating films for pharmaceutical applications, in which the permeants of interest are usually larger molecules, such as proteins, DNA, or other high molecular weight active substances. Such molecules will have significantly slower diffusion through the film than the solvent molecules, which as a result might induce osmotic pressure differences between the cells. Nevertheless, this phenomenon, while present, is not that important as long as the molar concentrations of macromolecules are relatively small, and salt is added to screen potential charges on the macromolecules i.e. the effect of the counterions release is negligible.

3. Permeability over different film structures

This part will summarize the literature on specific studies where the permeability has been measured by either modified Ussing chambers or in side-by-side diffusion cells. The chapter is divided into different subchapters where the different structures presented in Fig. 1 are discussed. However, the first section covers a general introduction of how a material and its structure might affect the permeability. Barrier films can be produced using a wide range of methods, such as solvent casting, extrusion, hot-melt pressing, spraying, spin coating, moulding, etc. Depending on the polymers and the process used for production, the structure of the final film can vary to a great extent. Possible structures can be non-porous (or dense), layered, composites, porous, and swelling materials, as shown in Fig. 1. The permeability P is according to Eq. (5) equal to the partition coefficient K times the diffusion coefficient D. In general, the barrier properties of a polymer will depend on the chemical structure of the polymer as well as the permeant, and in addition, the mobility of the polymers. The chemistry of the polymer is however the main defining factor determining the barrier properties, for example, the permeability can be tuned by six orders of magnitude by grafting chemical side groups to the polymer chain solely, mainly due to disruptions or by densifying the material structure depending on the nature of the grafted chain [44]. Furthermore, the chemical interactions between the permeant and the material are of importance and will have an impact on the permeability of the material, as well as the environment including the solvent, the temperature, and the pressure. The solvent may at the extreme cause dissolution of the films, but even in less extreme cases, swelling or plasticization can greatly impact the transport through the film. An increased temperature will also affect the polymeric material, which for example, can undergo a transition from a static glassy state to a more dynamic rubbery state when the temperature is higher than the glass transition temperature of the polymer. The temperature will further impact the chemical potential of the permeant, and an increased temperature will also increase the

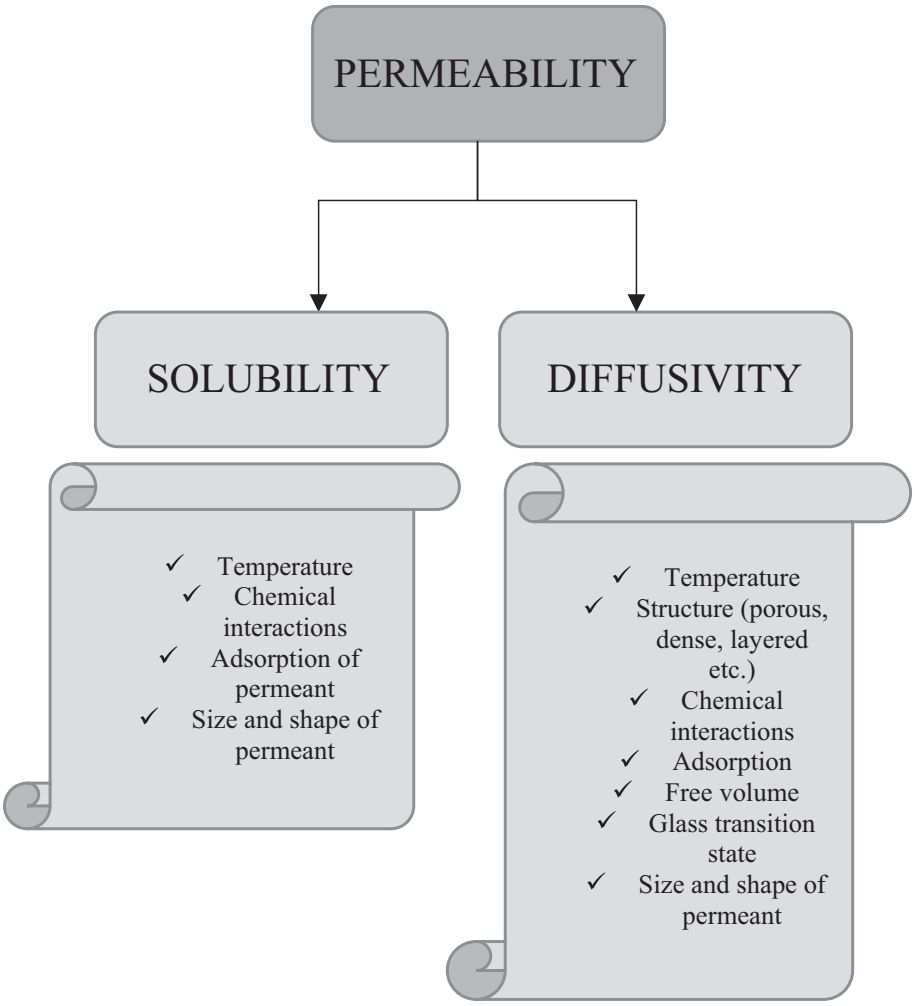

Fig. 4. Summary of the factors that affect the permeability, classified in solubility and diffusivity.

molecular motion of the polymers in the barrier films. In general, an increased temperature results in an increased permeability since it affects both the solubility and the diffusivity.

Fig. 4 aims to summarize the different factors that affect the permeability as well as providing the reader with an overview. The partition coefficient (also denoted the solubility coefficient) basically demonstrates *how prone the permeant is to dissolve into the polymer relative the concentration in the surrounding media*. The latter is affected by the chemical structure of the permeant, as well as the chemical structure of the polymer. Two mechanisms can be defined by which a permeant displace through a polymeric film: (i) dissolution in the polymer phase constituting the film and diffusion in the amorphous polymer network, and (ii) diffusion in liquid-filled pores. In many cases the displacement of the permeant will in fact be a combination of both, for example, even in porous films where the main transport is assumed to be through the pores, it might also be transport through the solid polymer phase. In addition, during the initial wetting stages, liquid may progress through the film through wetting of the interfaces and capillary forces. By taking the two main mechanisms into consideration, it is obvious that the size, the shape, and the chemistry of the permeant will have an impact. For example, permeants with longer chain lengths have been shown to have lower solubility than shorter permeants in cross-linked polystyrene [45]. However, a smaller molecule is expected to have an increased mobility. As mentioned above, the shape of the permeant is also an important factor and for example, elongated molecules have higher diffusion coefficients than spherical molecules of equal molecular volume [46,47]. The latter has been explained by the orientation of the anisotropic molecules along their longest axis [46]. Furthermore, it has been hypothesized that a larger molecule permeant is more prominent in plasticizing the polymeric barrier than a smaller permeant [48]. A permeant that is soluble in the polymer can induce swelling of the material, which results in increased permeability due to the plasticizing effect. Plasticization of the barrier increases both the diffusivity and solubility of a permeant, and increases the mobility of the polymer chains, which all together contributes to an increased permeability of the barrier. Adsorption of the permeant to the film surface, when utilizing diffusion cells, might be an obstacle and result in an overestimated permeability [49], which is due to the changed equilibrium between the donor chamber and the film surface. In the latter the partition coefficient will increase due to the higher amount of the permeant on the surface.

The microstructure of the barrier film will have a large impact on the permeability and can be divided into four categories: (a) the porosity, (b) the film microstructure, (c) the polymer morphology, and (d) the chemical structure. For example, a porous film (a) is expected to have a higher permeability than a dense or a composite film, since the transport is expected to be faster within the pores, whereas (b) the final film microstructure is often affected by the manufacturing process of the barrier material due to the fact that many polymers are immiscible, which might result in phase-separation of polymer mixtures. The morphology of the polymers (c) also affects the permeability since amorphous and crystalline parts have different permeability [8], and in addition, increased ordering of the polymer chains also decreases the permeability [49]. Finally, (d) the chemical structures influence the free volume, and for dense polymeric materials, the free volume will be the most important factor for the permeability (see Eq. (8) below). The free volume is constituted of the micro-cavities present in a polymeric material that the permeants can use to diffuse through the barrier [20,23,24]. The free volume is strongly related to the chemistry by the cohesive energy density, but also to properties such as thermal history, glass transition temperature, crystallinity, and conformational order.

The diffusion of a permeant is suggested to only occur in the amorphous part of semi-crystalline polymers where the cohesive energy density is low, and the amount of free volume is high. Diffusion between the voids of free volume can be considered as jumps, and the diffusion then depends on the probability of a permeant to find an adjacent free volume [23]. An example of such material is high-density polyethylene (HDPE), which has been shown to have low gas permeability due to the low fractional of free volume.

The glass transition temperature is relevant for the barrier properties, and the largest effect will be observed if the polymer is above (rubbery), or below (glassy) its glass transition temperature. In general, the diffusion is faster in a polymer in its rubbery state, even if there are examples that shows the opposite [23].

The interfaces formed between materials (both miscible and immiscible) may have other properties than those of the bulk, and should be taken into consideration regarding the formation of structures and properties of barriers [65]. The presence of filler in a barrier material will also have an impact on the permeability, especially if the filler is impermeable, which will cause a so called tortuosity path i.e. a longer transport path since the permeant has to go around the filler. [8,32,33]. However, it is important to consider the compatibility between the filler and the matrix. A poor compatibility may result in voids and channels at the interface. Such channels can then mediate unhindered and rapid transport of the permeant, which greatly reduces the barrier properties as a result. In contrast, when the matrix and the filler are highly compatible, no voids are formed, and the presence of the largely impermeable filler is expected to result in decreased permeability. Table 1 summarizes the different structures and the range of observed permeability, which are discussed in the following sections. Additionally, all structures will be further discussed with respect to the measurement setup with modified Ussing chambers or side-by-side diffusion cells (pros and cons).

3.1. Non-porous (dense) materials

The non-porous material in this review is defined as a solid and dense material, where the solution-diffusion model can be used to describe the permeability, i.e. the permeant needs to dissolve into the film surface before it can diffuse through, and finally diffuse into the acceptor chamber. In addition, the free volume within the film material will be of importance for the transport of permeant. The free volume theory is based on the matter in a material that is not occupied, and that rearrangements of these volumes makes it possible for the permeants and/or the solvents to move (or jump) through the material. This is the main reason why the permeant and the solvent can displace through the material as stated in the theory by Fujita in 1961 [20,66]. Fujita's model is based on a ternary system consisting of a solvent, a

Table 1
Summary of the materials that are compared and discussed.

Classification	Range of P (m^2/s)	Examples of applications	Studied system
Non-porous	$1{\cdot}10^{-13}$-$1{\cdot}10^{-17}$	Packaging, coating	LDPE [49] EAA [49] EC [21,50] Latex EC [51–53]
Laminates	$1{\cdot}10^{-14}$-$1{\cdot}10^{-17}$	Packaging	LDPE/EAA [49] PHB [54] Si/EVA [43]
Composites	$1{\cdot}10^{-12}$-$1{\cdot}10^{-13}$	Packaging, car interior	PLA/MCC [55] PLA/CNC [10] LDPE/CNC [56] PMA/Al [57] PP/CS [58]
Porous (constant and changed)	$1{\cdot}10^{-10}$-$1{\cdot}10^{-13}$	Coatings for controlled release	EC/HPC [16,18,59] PHB/PAA [54] EC/Eudragit [17,60].
Swelling	$1{\cdot}10^{-10}$-$1{\cdot}10^{-13}$		MFC/HPMC [39] CNC/HPMC [61] BPPO/polyNIPA [62]
Swelling porous	$1{\cdot}10^{-10}$-$1{\cdot}10^{-13}$	Coatings for controlled release	PHB/PAA [63] EC/HPC [21] EC/polyNIPA [62] MAA/polyNIPA [64]

polymer, and a permeant (a plasticizer), where the concentration of the plasticizer was kept low. Fujita suggests that the probability P (υ*) to find holes of sizes υ* that are of the same as for the permeant molecule is equal [66,67] to:

$$P(\upsilon^*) = A\, e^{\left(-\frac{b\upsilon^*}{f_v}\right)}, \tag{8}$$

where A is constant, b is a constant in the order of unity and f_υ is the average free volume per permeant molecule. The parameters bυ* have been interpreted as the minimum size for a displacement of the permeant and the probability $P(\upsilon^*)$ to find holes with a certain size υ* is also closely linked to the size of the molecule, and thereby, the mobility of the permeant. The model correlates well to systems which consist of polymers and organic solvents, while it fails to describe systems that include water. The latter is due to numerous interactions between the molecules [20], and the model has been further developed to increase the correlation between the diffusion of relatively small permeants in dilute and semi-dilute polymer systems [68].

Additionally, Vrentas and Duda have also developed a model, which is applicable under varying temperatures and polymer concentrations [69–72]. A drawback with this method is that 14 (!) different parameters are needed in order to predict the self-diffusion coefficient, out of which 10 has to be evaluated [73].

Bolton and coworkers have developed a mathematical method based on Monte Carlo and molecular dynamic simulations for calculation of diffusion and solubility coefficients of water and oxygen of low-density polyethylene (LDPE) films, which are in good agreement with experimental data [74]. The diffusion is expected to occur due to jumps within the polymeric material.

Regarding the permeability measurements in modified Ussing chambers, the measurement time may vary between a couple of days to several weeks or even months, depending on the material and the permeant [21,49,50]. For example, for a pure film of LDPE, the permeability of water and acetic acid is equal to $2.5{\cdot}10^{-15}$ m^2/s, which has to be measured over several weeks or even months [49]. Oleic acid on the other hand has a much faster transport in LDPE and EAA (see Fig. 5a), and a pseudo-steady state is reached within a week. This phenomenon is partly explained by the adsorption of the permeant to the film surface during the experiment, whereas another possible explanation could be that the partition coefficient is higher for oleic acid than acetic acid in the two plastics. Fig. 5b shows the permeability of water and the model drug of theophylline in films of ethylcellulose (EC), where the manufacturing process has been different. A pure EC film has a water permeability in the range of $0.6–2.3{\cdot}10^{-12}$ m^2/s [21,50], which can be measured within a couple of hours.

Non-porous films can also be produced from dispersions of free particles, as schematically shown in Fig. 6a-b, either by solvent casting, or spray coating. In both cases, it is important that the particles coalescence to achieve dense and solid films. Kazlauske and coworkers measured the water permeability as well as the permeability of a model drug (Theophylline) of films produced via spray coating [52]. The films showed a higher permeability to water ($27{\cdot}10^{-13}$ m^2/s) than the model drug ($3.2{\cdot}10^{-13}$ m^2/s) (see Fig. 5b), which most probably is a result of the different chemical structures and the sizes of the permeants. Additionally, the plasticizing effect of the model drug was evaluated, but the water permeability was more or less constant ($19{\cdot}10^{-13}$ m^2/s) [52]. When studying the cross-sections of the films using SEM, it was observed that the coalescence was not perfect, i.e. particles were noticeable. This was even more obvious after the exposure to water, where individual latex particles could be observed in the structure and resulted in smaller micro voids (nm- to μm scale), which could influence the mass transport properties, and thereby a higher permeability than expected.

3.2. Laminates

Layered materials are present in many daily products ranging from packaging materials to wound care products, and diapers. In these products, the transport of water and other liquids are crucial for designing products with desired properties. By knowing the mass transport through each individual layer, it should be possible to calculate the theoretical permeability for a layered material according to Eq. (9):

$$\frac{h_{tot}}{P_{tot}} = \sum_1^n \frac{h_i}{P_i} \tag{9}$$

where h_i is the thickness, and P_i is the permeability of the individual layers, respectively. The expression assumes that the mass transport dm/dt is equal through each layer and that steady state has been reached [75,76]. Furthermore, it is assumed that the mass transport is constant regardless of the order of the defect-free individual layers.

In an experimental study, laminates consisting of two, four, and eight layers had a decreased permeability of both oleic and acetic acid than the pure film materials (LDPE and EAA) (see Fig. 7) [49]. The

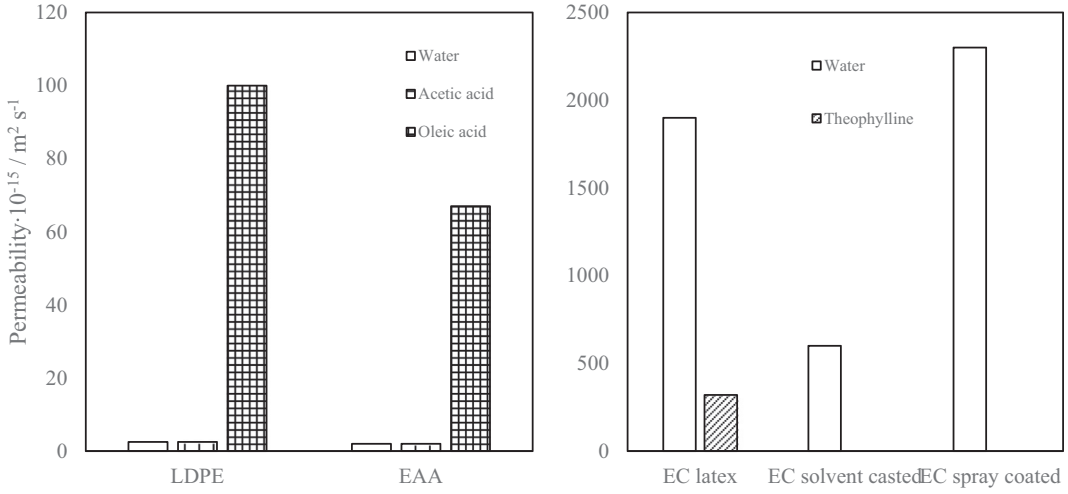

Fig. 5. Data adapted from references [49,52] for left and right in the Figure, respectively, shows a summary of the permeabilities of (a) water (open), acetic acid (stripes) and oleic acid (chequered) in the two common plastics LDPE and EAA, and (b) the permeability of water (open) and the drug molecule Theophylline (chequered) in ethylcelluose, EC, films produced by casting of an EC latex suspension or casting a solution of EC dissolved in ethanol or the same EC solution but spray coated. Please notice the scales on the y-axis.

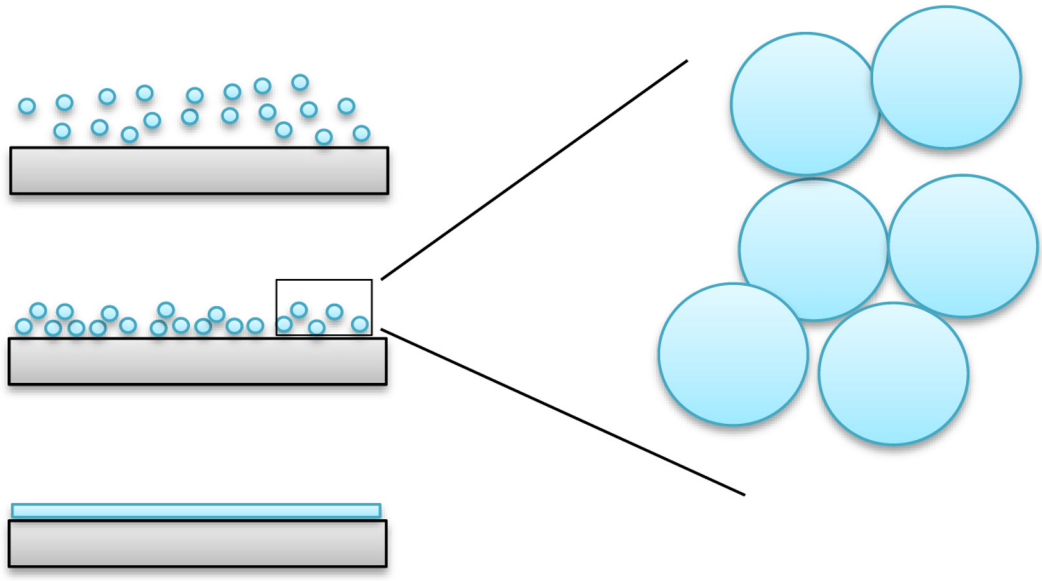

Fig. 6. (a) Production of films via coalescence of particles in a dispersion, and (b) enlargement of the coalescence.

number of layers did however seem to have a small impact on the permeability of both oleic and acetic acid, which was explained by the ordering of polymer chains close to the interface. The latter was confirmed using SAXS and WAXD to study the crystallites in the interface. The hypothesis is that the ordering close to the interface functions as a hinder of the two carboxylic acids, which affects the permeability.

Bergstrand and coworkers combined a non-porous layer with a porous layer and measured the water permeability. The solid non-porous layer corresponded to only one-tenth of the total film thickness, but the permeability decreased to values similar to a completely non-porous film, indicating that it was the latter that solely determined the total water permeability [54].

Liang and Siegel produced laminates of silastic and ethylene vinyl acetate copolymer and measured the permeability of salicylic acid in side-by-side diffusion cells [43]. They showed that the partition coefficient of salicylic acid was higher while the diffusion coefficient was lower in the ethylene film compared to the silastic film.

3.3. Composite materials

A composite material consists of two or more different constituents, typically denoted matrix and filler. The matrix is the continuous phase that surrounds the fillers, which should enhance the properties of the matrix material. The transport properties of a composite material can be estimated using the effective medium theory for the matrix and the fillers. For more general overview over the effective medium theory the reader is referred to books by Christensson [77] or Chok [78]. Applying effective medium theory on the diffusion transport in composite materials with impermeable filler gives:

$$D = \left(1 - \frac{3}{2}\Phi_{filler}\right) D_{matrix} \tag{10}$$

where ϕ_{filler} is the volume fraction of filler and D_{matrix} is the diffusion coefficient for the permeant in the polymer matrix. Eq. (10) elucidates that this theory predicts that the amount of filler is slowing down the transport rate. This can be interpreted as that the increased amount of filler give increased tortuosity and that this is considered as the major factor affecting the permeability, and there are several possible transport paths for a diffusing molecule through a composite material (see Fig. 8). The shape and the aspect ratio of the filler affect the diffusion, but several other factors including the solubility in the matrix and filler, the dispersion, the adhesion to the matrix, the filler-induced solvent retention, and the induced porosity [65,79,80] are also of importance Fig. 8 shows schematic images of how fillers can affect the transport path through a composite: more specifically Fig. 8a shows the average tortuosity path through a polymer matrix without any added filler, Fig. 8b shows the transport path when the added fillers are perfectly aligned, and Fig. 8c, in which the fillers are randomly oriented, shows another example of the increased tortuosity caused by the presence of fillers.

Filler materials may also function as nucleating agents and can induce crystallinity in the matrix polymer [23,81]. Filler-induced crystallinity increases the volume fraction of regions with very low diffusion coefficients, and may thereby increase the tortuosity path, which leads to slower diffusion processes, and consequently, to a reduced permeability [65,82,83]. Another possibility is that the interface is a more favourable environment for diffusion than the bulk matrix due to surface modification, with poor adhesion, which results in cavities or pore formation [23,56,84], that causes faster diffusion and hence, increased permeability. Therefore, it is important to be able to predict the permeability to control the filler matrix interactions. Additionally, the amount of added filler is important when it comes to percolation theories. For a filler in the micrometer scale a higher amount of filler can be added compared to a filler in nano-scale, where the percolation threshold only is a few percent, depending on the size and shape.

Theoretical approaches often consider fillers as impermeable non-overlapping particles, and assume no permeability changes in the polymer matrix [8,9]. The permeability for such systems, where the fillers are completely aligned, was first calculated by Nielsen in 1967 [8]. Here, all filler particles were aligned with their larger surface parallel to the film surface, creating longer tortuosity paths for the diffusing molecule, and the contribution to the composite permeability was derived to (Eq. (11)):

$$\frac{P_{comp}}{P_{poly}} = \frac{1-\Phi}{1+a\Phi} \tag{11}$$

where a is the aspect ratio of the filler and ϕ is the volume fraction of the filler [8]. In 2001, this model was further developed to account for

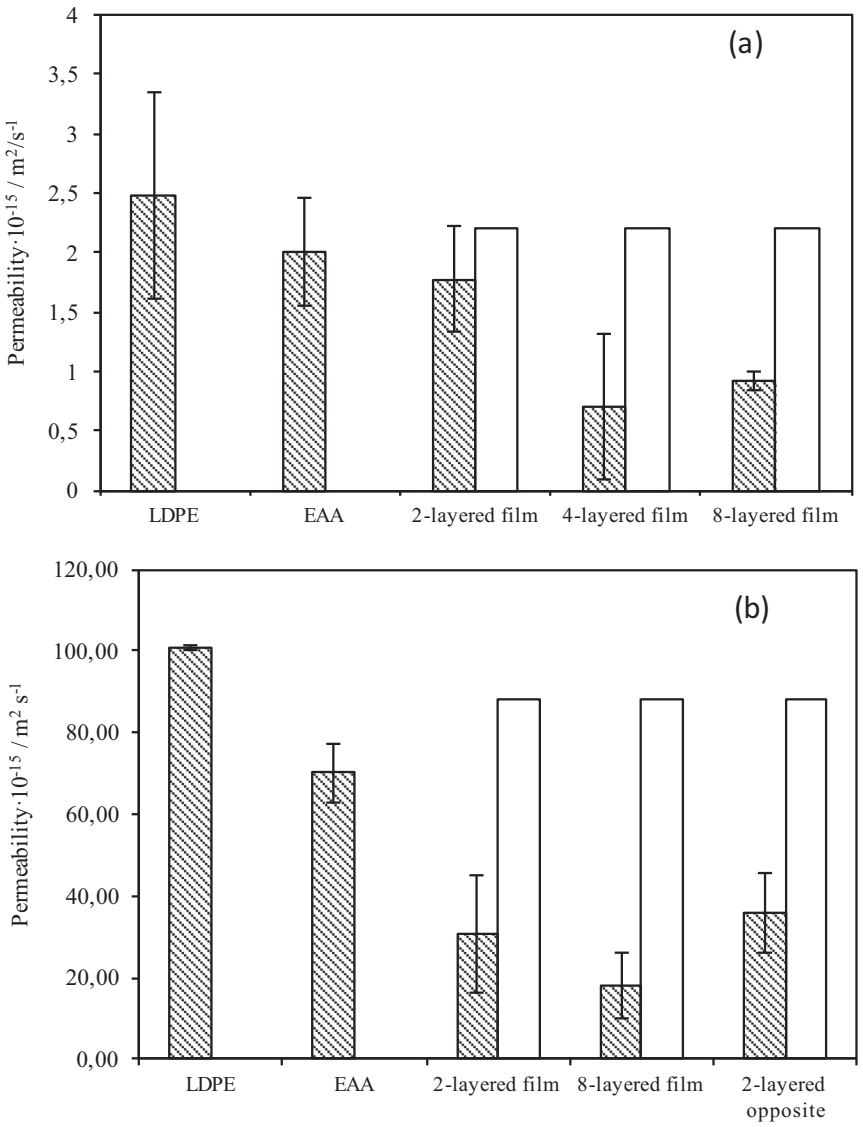

Fig. 7. Permeability of (a) acetic acid and (b) oleic acid, in plastic dense films and layered film materials. Grey values are experimental data and white bars are theoretical values calculated from Eq. (11), which assumes that the interfaces have no impact on the total permeability. As also can be seen in the figure, the permeability of a 2-layered film was equal, independent of which surface that was facing the donor chamber.

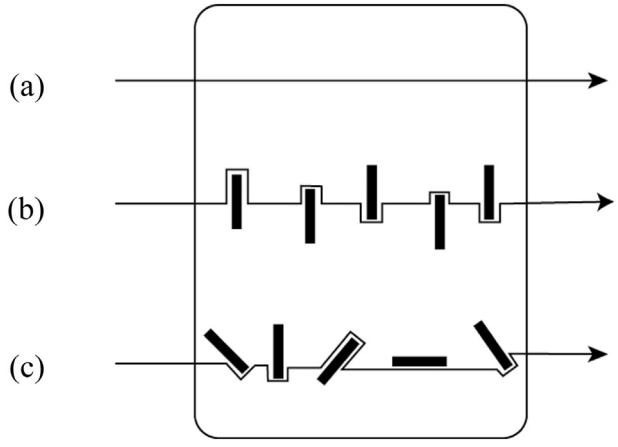

Fig. 8. Schematic image of how fillers can affect the transport path through a composite: (a) pure matrix, (b) perfectly aligned fillers, and (c) randomly aligned fillers [41].

non-aligned fillers by introducing an order parameter *S* for the filler orientation:

$$\frac{P_{comp}}{P_{poly}} = \frac{1-\Phi}{1+a\Phi\frac{2}{3}\left(S+\frac{1}{2}\right)} \tag{12}$$

Eq. (12) reduces to Nielsen theory for perfectly aligned fillers when $S = 1$. This equation has been further developed for randomly placed circular fillers [85], and the conclusion from all these theories is that perfectly aligned fillers will result in a lower permeability than randomly aligned fillers, if the aspect ratio of the filler is equal in the two cases [65]. Also 2D materials fillers such as graphene [86,87] have been introduced in composites, which has shown to reduce the permeability [88]. For random oriented platelets the permeability for the composites follows [89]:

$$\frac{P_{comp}}{P_{poly}} = \left(1+\frac{a^2\Phi}{1-\Phi}\right)^{-1} \tag{13}$$

Recently Nazarenko et al. [90] found that the permeability for stacks of platelets do not follow these simple approaches and Greco et al. used numerical simulations to study the effect of dispersion of the platelets [91,92].

Producing more sustainable materials, with biodegradable plastics such as polylactide acid (PLA) and poly(lactide-*co*-glycolide)(PLGA) have gained large interest [93]. In addition, cellulose, which is the world's most abundant renewable polymer [94], has several times been used as a filler in different composite materials [10,12,55,56,82,95–101] aiming to both strengthen the materials, and decrease the permeability. Unfortunately, the surface chemistry of cellulose is incompatible with most plastics [12,93,98–100,102], and to overcome this problem, there has been a large effort to modify the surface of cellulose [56,100–103].

Experimental results have shown that the theories of increased tortuosity paths are not always suitable. For example, nanocomposites consisting of either PLA or PLGA as matrix, and varying amounts of nanocrystalline cellulose (CNC) produced via solvent casting, resulted in an increased water permeability, in opposite to what is expected according to theoretical predictions, see Fig. 9a-b [10]. The pores were shown to be formed to a higher extent after the surface of CNC had been modified with PLA-chains, which in theory should have resulted in an increased compatibility between the matrix and the filler [10]. On the contrary, the pore formation was explained by an increased viscosity during the solvent evaporation as the composites where produced, which resulted in a locked network of the cylindrical fillers where the polymer could not precipitate homogeneously.

In a similar study by Gårdebjer and coworkers, the surface of CNC was modified with Y-shaped carbon chains of varying lengths [56], the modified CNC was added to a matrix of LDPE, and the water permeability was measured. From this study, it can be concluded that the agreement between the experimental results and the theory by Nielsen was depending on the carbon chain length, i.e. the longer chain gave a better correspondence, see Fig. 9c, which is probably a result of the increased compatibility between the matrix and the filler. In the case of unmodified CNC, the water permeability increased to a higher value compared with the pure LDPE film, which might be explained as a result of poor compatibility between the matrix and the filler. The theoretical values from Nielsen theory for randomly aligned fillers with an aspect ratio of 50 have been added for comparison with the experimental results.

Another possibility to increase the compatibility between cellulose and PLA is to use a hemicellulose, for example xyloglucan [93]. Composite materials of PLA, microcrystalline cellulose, and xyloglucan were produced via extrusion followed by hot-melt pressing, where the surfaces of the cellulose particles were covered with the xyloglucan prior to extrusion. The permeability studies of cellulose covered with xyloglucan and dispersed in PLA shows larger permeability than cellulose PLA composite, which was a result of the presence of the more hydrophilic hemicellulose located between the matrix and the filler. That water migration can be facilitated in the interface layer has also been shown for other systems, like pigments in water borne coatings [104].

An example of how chemical interactions between the permeant and the material can affect the permeability was shown by producing composite films of quaternary polymethacrylate (i.e. Eudragit RS and RL) with magnesium aluminum silicate [57]. The permeability of several model drugs was determined by using side-by-side diffusion cells, and since Eudragit contains positively charged ammonium groups, negatively charged SiO-groups could interact with these, and thereby the permeability could be controlled. A higher amount of ammonium groups resulted in a decreased permeability because of the formation of a denser composite material due to ionic interactions between the charged groups, which resulted in a decreased diffusion coefficient of the model drugs. Additionally, the authors also showed that the diffusion coefficient decreased with increasing molecular weight of the permeant.

3.4. Porous films

Porous materials can be created already in the film production, for example by using an emulsion-template [54], or by first producing a phase-separated material from which one of the phases can be extracted, i.e. in the case of release studies of an active ingredient in the pharmaceutical field [59,105]. Applications of interest are for example, coatings for controlled release systems, and by varying the ratio of two polymers with different characteristics, the final properties of the film coating can be controlled [17].

Porous films or coatings can be used when semi-permeable materials are needed. Many polymers are not miscible, which might result in a phase-separation where the two phases are enriched with one of the polymers. For example, when producing coatings for controlled release, ethyl cellulose (EC) and hydroxypropyl cellulose (HPC) can be dissolved in ethanol and films could be produced via spray coating [14]. The phase-separation might in this case occur already in the solution, and thereby, be used as a tool to create porous coatings. The final film often consists of a polymer matrix which is considered as impermeable, where the permeant can either be transported or diffuse in the water-filled pores, that has been created due to leakage of the water-soluble polymer.

Fig. 10 illustrates that porous films can display different microstructures of the pores, and that the connectivity is important for the permeability. For the above discussed EC/HPC system, it is clearly shown in Fig. 10d that an increased porosity results in an increased water permeability [106,107]. Already 1957 Broadbent and Hammersley presented the percolation theory of how a fluid could flow through a porous material if the porosity was above a certain level called the percolation threshold p_c: the volume fraction when the pore network becomes connected. [108] The larger the porosity is above the p_c, the larger degree

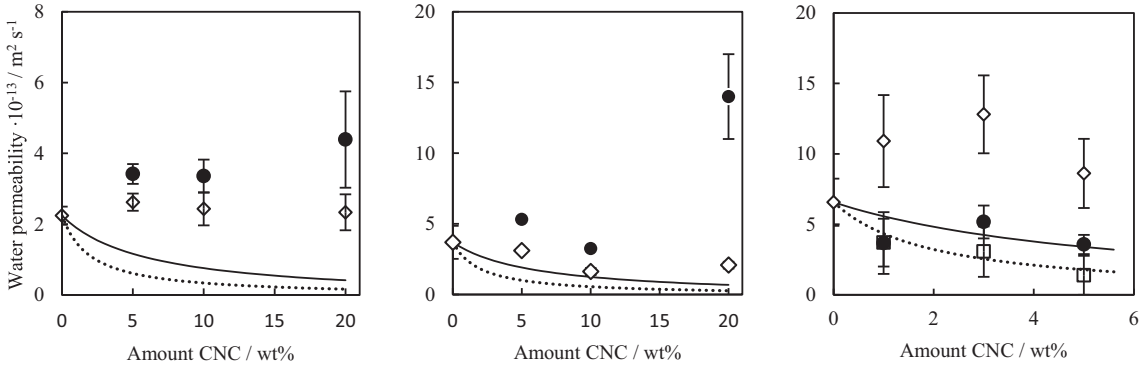

Fig. 9. Water permeability of composites of PLA and PLGA [10] in (a) and (b) and LDPE [56] in (c), where (◇) represents unmodified CNC, and (•) and (□) surface modified CNC. The theoretical values using Nielsen model with perfectly aligned cylindrical nano-fillers are plotted as a dashed line and the straight line shows random distribution, the aspect ratio was set to 50.

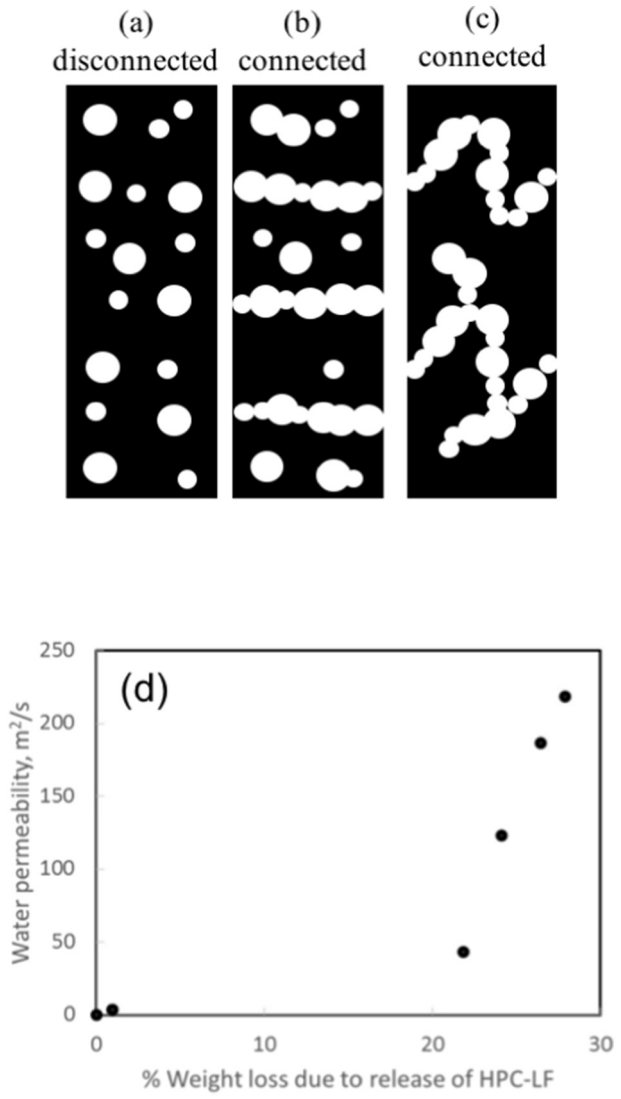

Fig. 10. Schematic images of porous films, where pores are (a) disconnected, (b) connected and forms a transport path through the material, (c) connected but having "dead-ends", and (d) where data from [95] shows how an increasing amount of released HPC-LF increases the water permeability.

of connectivity and thus permeability. For a deeper overview around percolation the reader is referred to ref. [109,110].

Lindstedt and coworkers have produced films of ethyl cellulose and hydroxypropyl methyl cellulose (HPMC), where the HPMC is expected to leak out from the film, leaving a porous skeleton [111]. The water permeability was measured, and as expected, to be lowest for the pure ethylcellulose film ($1.85 \cdot 10^{-12}$ m^2/s), while it increased upon adding an increasing amount of the pore forming agent HPMC. The highest water permeability was noticed for the film where 30% of HPMC had been added ($22.8 \cdot 10^{-12}$ m^2/s). For a similar system, containing EC but with HPC instead of HPMC, several aspects on the film microstructure and the permeabilities have been studied, for example a) ratio between EC and HPC, b) the molecular weight of the polymers in coating, and c) the manufacturing conditions.

a) Marucci and coworkers varied the amount of HPC from 20 to 30%, and found that the water permeability for films increased with more than an order of magnitude when the amount of increased from 22 to 26%, see Fig. 11d [112]. This could be related to the macrostructure and that phase-separation developed during the film formation. It was also shown that the pure EC coatings were semipermeable, letting water to be slowly transported through the film. However, for HPC contents exceeding 22% also the HPC leaching increased, from <5% to >20%, and that the water was transported mainly through the formed water filled pores. This indicates that the microstructures for films with HPC contents above 22% are connected, and it can be explained by that a phase-separation via spinodal decomposition was occurring [113]. Furthermore, it was also shown that films consisting of 24% HPC had a lag time of approximately 45 min, whereas it was 20 min for a film with 30 wt% of HPC [112]. The differences in lag time is correlated to the time it takes for the water soluble HPC to leach out, and hence, the final film structure to be formed. This is an important parameter to consider when designing pharmaceutical coatings for controlled release depending on the desired release profile. In a later study on drug release from EC/HPC systems, it was shown that the drug release mechanism was related to osmotic pressure for systems with minor HPC release (no pores available) [114] and diffusion of drug through the formed pores then HPC had been released and where available [112].

b) Andersson et al. have varied the molecular weight of EC or HPC in reference [59] or [16], respectively, while keeping the amount of EC (70%) and HPC (30%) constant. By varying the molecular weight of the water insoluble EC, they showed that the former has a large effect on the mass transport properties of both water and model drugs. The films consisting of EC with the lowest molecular weight resulted in films with the largest pores. The permeability of both water and mannitol decreased for the films with the largest molecular weight of the EC, which was explained by the fact that the phase-separation diagram depends of the polymers´ molecular weights, and that the phase-separation depends on the viscosity i.e. where higher molecular weights have larger viscosity and thus stops the phase-separation at lower dry contents. Furthermore, it was shown that the geometry and tortuosity of the pores are also depending of the molecular weight. Not surprisingly, it was also shown that the larger molecule mannitol displayed a five times lower permeability than water, which was interpreted to be due to larger steric hindrance for the larger molecule.
The same group was also varying the molecular weight of the water soluble HPC in films consisting of 70% EC and 30% HPC, and where the films were produced via spraying [16]. In this case the phase diagram was altered so much that the film forming mechanism shifted from nucleation and growth for shorter molecular weight of HPC, to spinodal decomposition for larger molecular weight of HPC. This resulted in unconnected pores lower molecular weight, and hence, that slower water permeability was observed, while for the higher molecular weight of HPC, the pores became connected, which resulted in an increased water permeability.

c) In an initial study on varying manufacturing conditions Marucci et al. [15] it was shown that the time of the drying process gave rise to more progression of phase-separation, and hence, the water permeability decreased. This was explained as if there is an extended time for phase-separation to occur: larger domains of the water-soluble HPC might form. The probability that these larger domains are connected through the film increases, and hence, a channel for water transport has been formed. In another EC/HPC study [115] with two different molecular weights of HPC, a variety of spray rates were compared, Andersson and co-workers showed that the same manufacturing conditions could result in a 15 times difference in release rate. This was related to the developed microstructures during film formation that appeared due to different paths (nucleation and growth or spinodal decomposition) of film formation that occurs during the drying of the coating droplets.

The Ussing chamber or side by side diffusion cells have also been used to study the effect of pores for other systems than EC/HPC spraying. For example, Adersjö and coworkers produced films of a

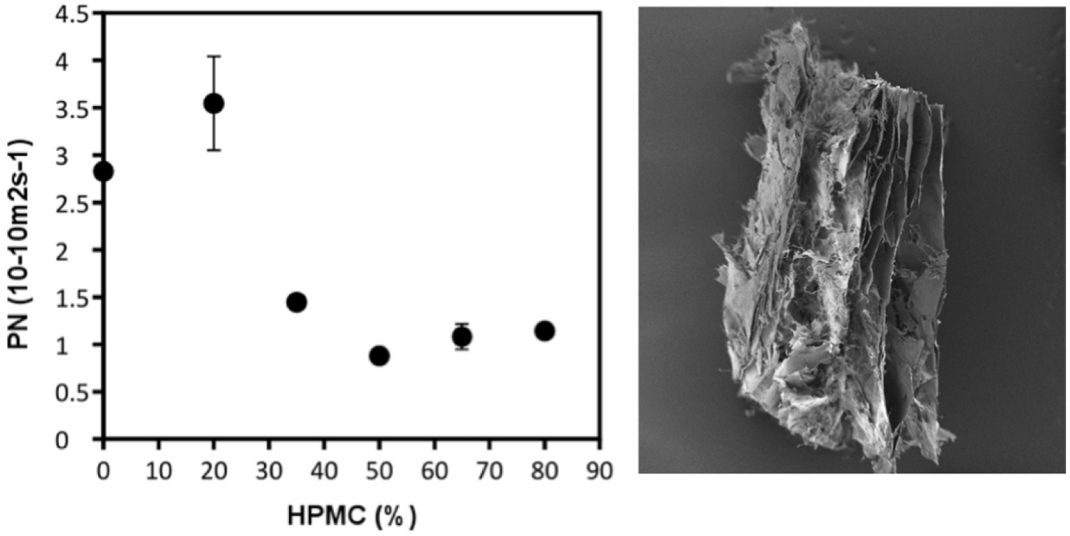

Fig. 11. Permeability and exemplifying structure of swollen MFC–HPMC films, to the left: Permeability normalized versus initial film thickness decreases with increasing amount of leachable, pore-forming HPMC, and to the right: SEM image revealing the layered structure and one-dimensional swelling that causes the permeability to decrease, even though the pore volume increases. Adapted from Larsson et al [39].

polymer dispersion Kollicoat SR 30D (a latex consisting of poly(vinyl acetate and poly(vinyl pyrrolidone), and sodium dodecyl sulfate), and combined it with chitosan, dextran, and/or, PEG600 [116]. Microscopy studies revealed poor coalescence of latex and porous films consisting of latex and chitosan, and thus an increased water permeability determined by Ussing chamber than the pure latex films. Mixtures of PEG600 and dextran added to the latex dispersion resulted in a phase separated structure during the drying of the coating, and domains of fused latex particles, and domains free from latex were observed. For these films, the initial times of the water permeability was in the same range as for the pure latex, whereas after approximately one hour, the permeability increased rapidly. This effect was explained with gradually dissolution of the solidified polymer network.

Cuppok and coworkers produced blended films of Kollicoat SR (poly (vinyl acetate) and Eudragit NE (poly(ethyl acrylate-*co*-methyl methacrylate), and measured the water permeability [60]. Kollicoat SR is more hydrophilic than Eudragit NE, and hence, the water permeability is expected to increase with an increased amount of Kollicoat SR. A combination of 90:10 Kollicoat, SR:Eudragit NE had a water permeability of approximately $70{\cdot}10^{-12}$ m^2/s, while it decreased to approximately $5{\cdot}10^{-12}$ m^2/s for a 50:50 blended film. The mass loss was increased for films with higher amounts of Kollicoat SR, which indicates a more porous film after exposure to water and agrees well with increased water permeability for more porous films.

Lecomte and *co*-workers produced films of gastrointestinal tract insoluble and enteric polymers EC and Eudragit L, respectively [17]. The aim was to create films where the drug release rate was low at low pH and gave an increased drug release rate by dissolution of the enteric polymer in the film at the pH (pH = 7.4) in the intestinal. This result was achieved in the paper, and a similar trend was confirmed by permeability measurement in side-by-side diffusion cell measurements of the model drug propranolol HCl at pH 7.4. Interestingly, free standing film experiments for 50:50 mixtures between the polymers showed <10% film weight loss in pH 7.4, whereas the propranolol permeability had increased remarkably. Furthermore, they also used Fick's second law to calculate the drug permeability and showed that the higher amount of the enteric polymer in the film increased the drug permeability, as expected.

Using leaching for the creation of a porous film material is not always appropriate, and another possibility to produce porous film materials is to use an emulsion template of varying compositions. Bergstrand et al. produced films of poly(3-hydroxybutyrate) (PHB) using an emulsion template of 3, 6, 8, 9, and 10% water were produced via solvent casting [54]. The films with three and six percentage water gave rise to pore sizes between 0.5 and 1 um, while the corresponding numbers for films with a higher amount of added water was 1-3um. Larger pores and porosities did also result in higher water permeability. Pure PHB films showed water permeability of $3.7{\cdot}10^{-13}$ m^2/s, while a permeability of approximately $900{\cdot}10^{-13}$ m^2/s was observed for the 10% water emulsion films, where the percolation threshold was between 8 and 9% water emulsion.

3.5. Swelling films

Permeability measurements of swelling films using Ussing chamber or side-by-side diffusion cells are difficult to perform due to the change in diffusion pathway. The examples below using these techniques can be seen as an inspiration of how to prepare swelling films. Furthermore, the impact of swelling on the transport through the films are discussed. The most common approach is to mix one swelling component with a material that does not swell. Different triggers, like temperature or pH, can be used to control the swelling, and thus the permeability of the films. In addition, the carrier material can be constituted of a polymer matrix or a fibrous network.

The swelling superabsorbent poly(acrylic acid) (PAA) mixed with the highly crystalline polyhydroxybutyrate (PHB), which is a pharmaceutical approved polymer that degrades slowly, was shown to form a hollowed swelled film after water exposure and swelling [63]. This because PAA is an anionic polyelectrolyte that has the capacity to swell hundreds of times their dry weight. Larsson et al. produced films consisting of PHB consisting of up to 25 wt% of PAA by solvent casting [63]. The water permeability was more or less constant for the films containing <15 wt% of PAA, and also similar to the water permeability observed for the pure PHB film ($6.6{\cdot}10^{-13}$ m^2/s). However, for films containing 15 and 25 wt% of PAA, the water permeability increased significantly ($1.5{\cdot}10^{-11}$ m^2/s and $8.2{\cdot}10^{-11}$ m^2/s respectively). This was explained by the lack of connectivity between the pores in the films with lower amount of PAA added, while the pores started to connect at higher amounts PAA, the latter was also confirmed from SEM images.

Triggered swelling can be obtained by using the polymer poly (N-isopropylacrylamide) (polyNIPAAm), which is a well-studied and a prominent temperature-responsive polymer. If cross-linked, the polyNIPAAm forms a hydrogel that shrinks or swells depending on if the temperature is varied above or below its transition temperature.

Several studies have focused on measuring the permeability in varied temperatures, and some studies also include chemical modifications, which makes the membrane pH-responsive. For example, Zhang and coworkers produced grafted membranes of polyNIPAAm and charged bromomethylated poly(2,6-dimethyl-1,4-phenylene oxide) (BPPO) [62]. The permeability of sodium salicylate was measured in side-by-side diffusion cells in deionized water at three different temperatures, 25, 37, and 43 °C. In this study it was shown that the permeability of the model drug increased with increasing temperature. This was explained by the higher hydrophilicity caused by the amination and charges.

Zhang and Wu incorporated polyNIPAm-*co*-MAA nanoparticles in an ethylcellulose membrane and the permeability was measured in side-by-side diffusion cells for several permeants [117]. They showed that the percolation threshold of the dry nanoparticles was between 20 and 30 wt% by measuring the permeability of Vitamin B12, and that the temperature dependence of the permeability increased upon increased temperature, due to the swelling of the nanoparticles. By the addition of MAA into the nanoparticles, they also made the membranes pH-responsive, and claimed that the temperature- and pH-responsiveness can be varied depending on the ratio of polyNIPAm:MAA. Additionally, they showed that the permeability decreased upon increasing the molecular weight of the permeant using different peptides and proteins, and they explained the decreased permeability as a size exclusion mechanism. In a similar study, Aliabadi and coworkers produced temperature- and pH-sensitive nanoparticles of NIPAAm and poly(methacrylic acid) (MAA), which were incorporated in a matrix of ethylcellulose by solvent casting technique [64]. The permeability of the anti-cancer drug doxorubicin was measured in side-by-side diffusion cells. They showed an increased permeability at increased temperatures and decreased pH, as expected for the temperature triggered swelling of NIPAAm.

Baker and Siegel produced hydrogels of NIPA:MAA:EGDMA in a ratio of 90:10:1, and measured the transport of glucose in side-by-side diffusion cells. In this study, a pH-gradient across the hydrogel was included, and it was shown that the flux could be controlled by decreasing the pH value [118]. Misra and Siegel developed the system where the pH during a permeability measurement could be varied [42]. This is especially interesting for pH-responsive hydrogels, which could have potential use for example as sensors, controllable membranes for separations, and drug delivery. They showed that the transport of the model drug benzoic acid could be varied across an ethylene vinyl acetate membrane at low concentrations.

In a study by Larsson et al. fibrous nanocellulose was mixed with swelling superabsorbents [119,120] or cellulose derivatives [39,61]. The nanocellulose films of microfibrillated cellulose (MFC) were produced via solvent casting, and different amounts of the cellulose derivate HPMC was added (up to 80 wt%) [39]. Thereafter the water permeability was measured for three hours for films, which consisted of <50 wt% of HPMC. In the case of >50 wt% HPMC, the films were fragile, and the permeability could only be measured for one hour before breaking. The pure microfibrillated cellulose (MFC) film showed a water permeability of approximately $3.0{\cdot}10^{-10}$ m^2/s, similar to a film which consisted of 20 wt% HPMC, whereas when higher amounts of HPMC was added, the water permeability significantly decreased (Fig. 11a). This could be explained by an anisotropic swelling of the films in the z-direction only, as seen in Fig. 11b, which consisted of >35 wt% of HPMC, and consequently resulted in a layered form of structure where the tortuosity path for the permeant was increased.

In a similar study, Johnsson and coworkers studied the swelling of a film, which consisted of nanofibrillated cellulose (NFC) or nanocrystalline cellulose (CNC), both combined with HPMC [61]. The main difference between the two studies is the aspect ratios of the different celluloses, where the CNC show lengths in the nanometer scale, whereas NFC and MFC show lengths in the micrometer scale. The films were produced by spray coating, and the films consisting of NFC and HPMC showed a similar anisotropic swelling as the films in the study performed by Larsson and coworkers. This was not the case though for the CNC-HPMC films, where the water permeability was shown to decrease independent of the amount added HPMC, and in the same range as observed for MFC-HPMC. The different behaviour of swelling and mass transport for water was explained by the difference in length scales of the used fibers, where for example, the longer NFC fibers shows a higher resistance to deform, which leads to a hindrance in swelling, and hence, a higher water permeability than the CNC films.

In recent years, regulatory authorities within pharmaceuticals have expressed their concern of the mixture of alcohol and extended release formulations, since the risk of dose dumping is increased if the dosage form is taken with alcohol [22]. It has been shown that the permeability of HPC-EC films showed a complicated dependence on the presence of alcohol in solution [21]. In the case of low amounts of HPC (i.e. <20%) in the films, the pores were not connected, and the permeability thus increased in the presence of ethanol as EC phase became swollen, with increased diffusion in the EC as a consequence. When the films contained >30 wt% of HPC the percolation threshold is reached, which resulted in decreased permeability due to a swelled EC matrix in 40% ethanol, see Fig. 12.

On the contrary, it has been shown that films of regenerated cellulose have lower permeability of acetaminophen in solutions with increasing amount of ethanol [121]. The membranes were expected to swell prior to measurement, while the thickness was assumed to be constant through the permeability measurements. The films showed a higher solvent uptake in water than in ethanol, and it was shown that the permeability coefficient of acetaminophen decreased when the concentration of ethanol increased. This was explained by the hydration followed by plasticization of the cellulose films in presence of water.

4. Simulation and mathematical modelling

In this last section, we aim to illustrate the use of mathematical modelling as a tool to increase the understanding of what influences the transport through a film. The reader should notice, that this is not a complete review of modelling efforts, it is rather meant to provide ideas of possibilities and future aspects. The transport of solute molecules through diffusion in a solvent is governed by the diffusion equation (or Fick's second law):

$$\frac{\partial c}{\partial t} - \nabla\cdot(D(x)\nabla c) = 0 \tag{14}$$

which describes the evolution of the solute concentration $c(x,t)$ in space and time, given a diffusion coefficient D, which may vary in space. The local diffusive flux is given by $j = -D(x)\nabla c$.

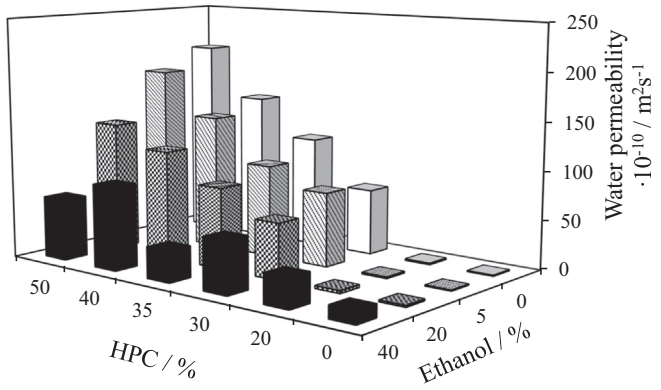

Fig. 12. Water permeability of EC:HPC films, where the amount of ethanol in the chambers was varied between 0 and 40%. The amount of HPC was varied between 0 and 50 wt%. Data from Larsson and coworkers [21].

We may discern two distinct cases of diffusion models through a film. In the first case, the material structure itself is modelled as impermeable, and the diffusion is simulated in the pores of the film material, where $D(x) = D_0$ i.e. equal to the free diffusion coefficient of the solute in the solvent. In this case, Eq. (14) is coupled with a boundary condition on the material surface, modelling that there is no flux into the material, namely:

$$j \cdot n = 0 \tag{15}$$

where $\boldsymbol{n}$ is the outward unit normal on the surface. This model has for example been used when the transport through a film used for controlled release applications was studied using lattice Boltzmann simulations [122].

In the second case, the solute molecules are allowed to penetrate different regions of the film, where the local effective diffusion coefficient $D(x)$ may vary between the regions. This model was used for simulating diffusion through a phase-separated material where the diffusion coefficient varied between the two phases [123]. In that work, different solubility in the phases was also considered in the model. In this case, the flux must be continuous across face boundaries, and the local concentrations must obey Eq. (4) at the boundary, which may be achieved by computing the continuous quantity $T(x) = c(x)/S(x)$, where S is the local solubility, see [123].

In both cases, the effective diffusion constant can be computed from Fick's law, Eq. (14), as:

$$D_{eff} = -\frac{L}{\Delta c}\bar{J} \tag{16}$$

by solving Eq. (15) to a steady state with an applied concentration difference Δc across the material. The average flux $\bar{J}$ in the direction of the concentration gradient can then be computed and L is the size of the simulation box. The value of D_{eff} can then be used in for example Eq. (4) to compute the diffusive flux through an entire film. To illustrate this approach, we present some results where the second approach has been applied to a computer-generated composite material consisting of a matrix and polydisperse spherical filler particles with varying effective diffusion constant inside the particles. An example geometry is shown in Fig. 13. The volume of the particles follows a gamma distribution with mean 3600 voxels^3 and standard deviation 1138 voxels^3, and with a total volume fraction of either 10% or 20%. The length of the side of the cubic simulation box was 250 voxels.

The results of computer simulations using the lattice Boltzmann method [124], are given in Fig. 14a. As expected, the permeability of the structure decreases with the amount of filler added and with a concomitant decrease of the diffusion coefficient inside the filler particles. The limiting case when P_{filler} tends to zero corresponds to simulation case 1 for impermeable structures described above. Although the general behaviour of the permeability curves is more or less expected, the exact shape and dependence on the permeability ratio between filler and matrix would be difficult to predict. In Fig. 13, lines following the diffusive flux field are also shown. These can be interpreted as the average paths for molecules diffusing through the structure. It is displayed that the paths tend to avoid the filler particles, and that the flux is lower inside the particles. These two effects both contribute to the lower permeability of the structure.

One of the major advantages with simulations is that we may equally well assume that the spheres in Fig. 13 are pores, with a higher permeability than the surrounding matrix. The results for this case are shown in Fig. 14b. Here, the total permeability increases with the volume fraction of the pores and with the permeability ratio of pores versus matrix. As the permeability in the pores increases, the total permeability seems to approach a limiting value where diffusion in the pores is so fast that all the resistance to diffusion is found in the surrounding matrix. Further studies regarding the type of materials shown above could include changing the size distribution of the spheres, further variation in porosity, and varying the shapes of the fillers/pores. It would also be possible to extend the model, for example by introducing boundary layers where the adhesion between filler and matrix is low or adding effects like adsorption of the solute molecules. It should be noted that simulations could also be performed in real material structures obtained through suitable microscopy techniques [122,123]. In these cases, the material structure cannot as easily be altered, but instead

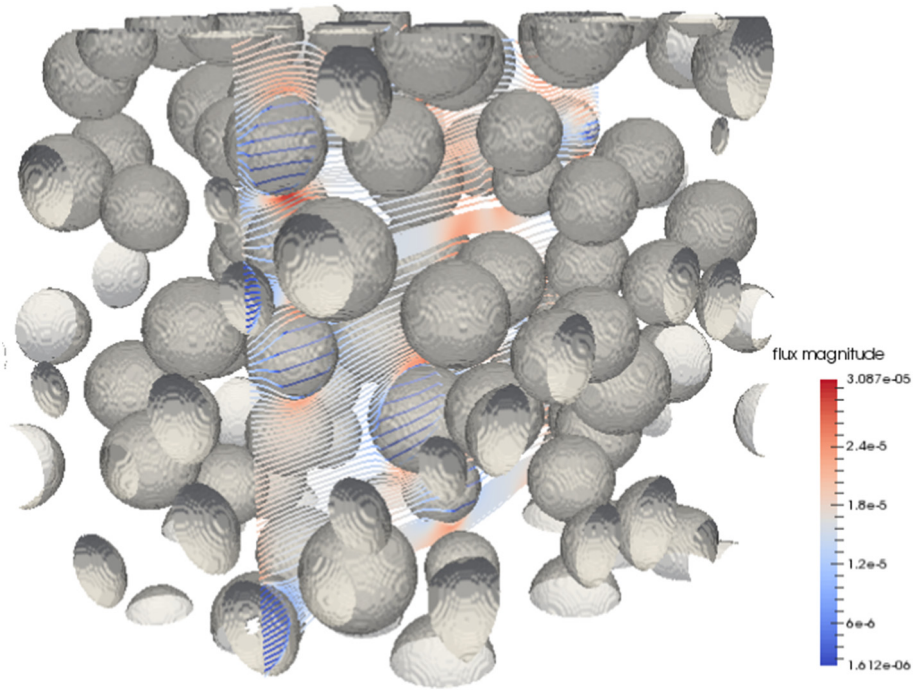

Fig. 13. A computer generated composite structure with spherical filler particles. The lines shown are flux lines following the local flux field and colored by the magnitude of the flux.

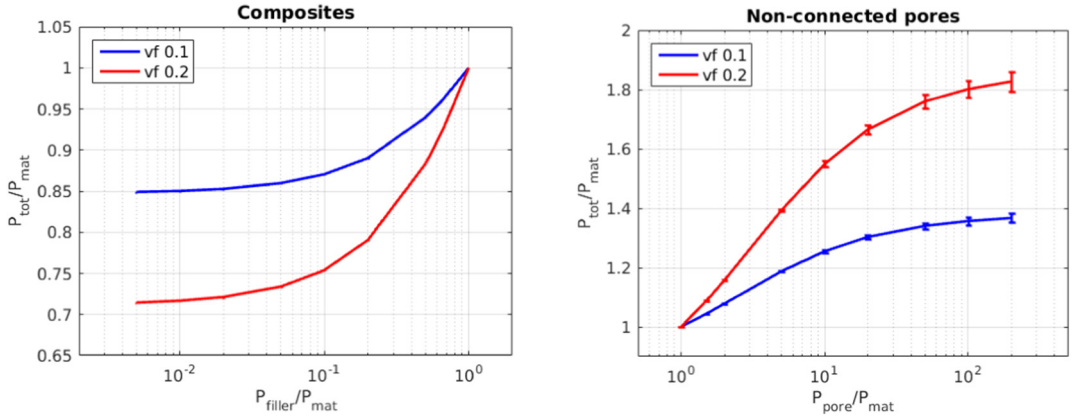

Fig. 14. Computed results for the permeability of the structure shown in Fig. 14. To the left for the case of a composite material, and to the right for a porous material, with 10 (blue) and 20 (red) vol-% fillers/pores. Each data point is the mean of results for three different geometries, and the error bars (which are barely visible in many cases) indicate the standard deviation.

analysis of the pore geometry in combination with diffusion simulations can provide explanations regarding what controls the permeability of the material.

The main advantages of the simulations presented here are that the results only reflect what is implemented into the model, and that input parameters, geometries, and other model input could be easily varied. While we have seen in previous chapters that there may be numerous factors influencing the transport through a film in complex ways, the simulations enable the study of how single factors influence the results. Thus, the simulations may help increasing the understanding of which effects are due to geometry, local permeability, or perhaps due to interactions between solute and material. Additionally, simulations of this type take minutes or hours to perform and can thus be performed on a large scale, while diffusion cell experiments may easily take days or weeks in addition to the careful preparation of samples, setting a limit to the number of measurements that can be performed. However, modelling and simulations should always be performed in parallel with experiments and results compared in order to make sure that no vital chemical or physical effects have been overlooked in the model.

5. Concluding remarks

Different manufacturing methods result in a variety of microstructures and permeability properties of films, barriers, and coatings. Altogether, the papers in the review confirm that there exists a strong correlation between the microstructure of the materials and the permeability of the permeant molecule. In addition, diffusion cells are shown to be a valuable experimental tool to achieve information about the permeability, as well as indications of the overall microstructures in the materials. Furthermore, we also show that computer simulations in combination with experiments can give a deeper insight about how geometry and local permeability influence the diffusion process. Hence, we strongly recommend this combination for future development of barriers, films, and coatings.

Acknowledgements

This work was part of the VINNOVA VINN Excellence Centre SuMo Biomaterials (2015-03150), which is also gratefully acknowledged for financial support.

References

[1] Borde A, et al. Increased water transport in PDMS silicone films by addition of excipients. Acta Biomater 2012;8(2):579–88.
[2] Vasile C, Pascu M, L. Rapra Technology. Practical guide to polyethylene. Shrewsbury: RAPRA Technology; 2005.
[3] Siepmann F, et al. Polymer blends for controlled release coatings. J Control Release 2008;125(1):1–15.
[4] Porter SC. Controlled-release film coatings based on ethylcellulose. Drug Dev Ind Pharm 1989;15(10):1495–521.
[5] Gerdeen J, Ronald R. Engineering design with polymers and composites. Vol. Second Edition. United States of America: CRC Press; 2012.
[6] Cussler EL. Diffusion barriers. Diffusion fundamentals, 6. ; 2007. p. 72.1–72.12.
[7] Kale G, Auras R, Singh SP. Degradation of commercial biodegradable packages under real composting and ambient exposure conditions. J Polym Environ 2006; 14(3):317–34.
[8] Nielsen LE. Models for the permeability of filled polymer systems. J Macromol Sci A Chem 1967;1(5):929–42.
[9] Bharadwaj RK. Modeling the barrier properties of polymer-layered silicate nanocomposites. Macromolecules 2001;34(26):9189–92.
[10] Gårdebjer S, Bergstrand A, Larsson A. A mechanistic approach to explain the relation between increased dispersion of surface modified cellulose nanocrystals and final porosity in biodegradable films. Eur Polym J 2014;57(0):160–8.
[11] Hossain K, et al. Physico-chemical and mechanical properties of nanocomposites prepared using cellulose nanowhiskers and poly(lactic acid). J Mater Sci 2012;47 (6):2675–86.
[12] Hietala M, Mathew AP, Oksman K. Bionanocomposites of thermoplastic starch and cellulose nanofibers manufactured using twin-screw extrusion. Eur Polym J 2013; 49(4):950–6.
[13] Piculell L, Bergfeldt K, Nilsson S. Factors determining phase behaviour of multi component polymer systems. Biopolymer mixtures. Nottingham: Nottingham University Press; 1995. p. 13–35.
[14] Marucci M, et al. Polymer leaching from film coating: effects on the coating transport properties. Int J Pharm 2011;411(1–2):43–8.
[15] Marucci M, et al. Effect of the manufacturing conditions on the structure and permeability of polymer films intended for coating undergoing phase separation. Eur J Pharm Biopharm 2013;83(2):301–6.
[16] Andersson H, et al. The influence of the molecular weight of the water-soluble polymer on phase-separated films for controlled release. Int J Pharm 2016;511 (1):223–35.
[17] Lecomte F, et al. Blends of enteric and GIT-insoluble polymers used for film coating: physicochemical characterization and drug release patterns. J Control Release 2003;89(3):457–71.
[18] Marucci M, et al. New insights on how to adjust the release profile from coated pellets by varying the molecular weight of ethyl cellulose in the coating film. Int J Pharm 2013;458(1):218–23.
[19] Häbel H, et al. Characterization of pore structure of polymer blended films used for controlled drug release. J Control Release 2016;222:151–8.
[20] Masaro L, Zhu XX. Physical models of diffusion for polymer solutions, gels and solids. Prog Polym Sci 1999;24:731–75.
[21] Larsson M, et al. Effect of ethanol on the water permeability of controlled release films composed of ethyl cellulose and hydroxypropyl cellulose. Eur J Pharm Biopharm 2010;76(3):428–32.
[22] FDA 2005, F.A.A.-P.I. 2005 [20161119].
[23] Lagaron JM, Catalá R, Gavara R. Structural characteristics defining high barrier properties in polymeric materials. Mater Sci Technol 2004;20(1):1–7.
[24] Koros WJ. Barrier polymers and structures. , Vol. 423Washington: ACS American Chemical Society; 1990.
[25] Siracusa V. Food packaging permeability behaviour: a report. Int J Polym Sci 2012; 2012:11.
[26] Wijmans JG, Baker RW. The solution-diffusion model: a review. J Membr Sci 1995; 107:1–21.
[27] Bernardo P, Drioli E, Golemme G. Membrane gas separation: a review/state of the art. Ind Eng Chem Res 2009;48(10):4638–63.

[28] Choudalakis G, Gotsis AD. Permeability of polymer/clay nanocomposites: a review. Eur Polym J 2009;45(4):967–84.
[29] Ussing HH. The active ion transport through the isolated frog skin in the light of tracer studies. Acta Physiol Scand 1949;17(1):1–37.
[30] Clarke LL. A guide to Ussing chamber studies of mouse intestine. Am J Physiol Gastrointest Liver Physiol 2009;296(6):G1151–66.
[31] Li H, Sheppard DN, Hug MJ. Transepithelial electrical measurements with the Ussing chamber. J Cyst Fibros 2004;3(Supplement 2):123–6.
[32] Crank J, Park G. Diffusion in polymers. New York: Academic Press; 1968.
[33] Krevelen DWv, Nijenhuis Kt. Properties of polymers - their correlation with chemical structure; their numerical estimation and prediction from additive group contributions. , Vol. 4Elsevier; 2009.
[34] Graham T. On the absorption and dialytic separation of gases by colloid septa. Phil Trans R Soc London 1866;156:399–439.
[35] Kushner Iv J, Blankschtein D, Langer R. Evaluation of the porosity, the tortuosity, and the hindrance factor for the transdermal delivery of hydrophilic permeants in the context of the aqueous pore pathway hypothesis using dual-radiolabeled permeability experiments. J Pharm Sci 2007;96(12):3263–82.
[36] Saripalli KP, et al. Prediction of diffusion coefficients in porous media using tortuosity factors based on interfacial areas. Ground Water 2002;40(4):346–52.
[37] Shen L, Chen Z. Critical review of the impact of tortuosity on diffusion. Chem Eng Sci 2007;62(14):3748–55.
[38] Peck KD, Ghanem A-H, Higuchi WL. Hindered diffusion of polar molecules through and effective pore radii estimated of intact and ethanol treated human epidermal membrane. Pharm Res 1994;11(9):1306–14.
[39] Larsson M, Hjärtstam J, Larsson A. Novel nanostructured microfibrillated cellulose–hydroxypropyl methylcellulose films with large one-dimensional swelling and tunable permeability. Carbohydr Polym 2012;88(2):763–71.
[40] Van den Mooter G, Samyn C, Kinget R. Characterization of colon-specific azo polymers: a study of the swelling properties and the permeability of isolated polymer films. Int J Pharm 1994;111(2):127–36.
[41] Gårdebjer S. Mass transport through polymer films: the importance of interfaces and compatibility. Gothenburg: Chalmers University of Technology; 2016.
[42] Misra GP, Siegel RA. Multipulse drug permeation across a membrane driven by a chemical pH-oscillator. J Control Release 2002;79(1–3):293–7.
[43] Liang W, Siegel RA. Theoretical and experimental exploration of rules for combining transport parameters in laminar membranes. J Chem Phys 2006;125(4):044707.
[44] Lagarón JM. 1 - Multifunctional and nanoreinforced polymers for food packaging. Multifunctional and nanoreinforced polymers for food packaging. Woodhead Publishing; 2011. p. 1–28.
[45] Kim D, Caruthers JM, Peppas NA. Penetrant transport in crosslinked polystyrene. Macromolecules 1993;26(8):1841–7.
[46] Berens AR, Hopfenberg HB. Diffusion of organic vapors at low concentrations in glassy PVC, polystyrene, and PMMA. J Membr Sci 1982;10(2–3):283–303.
[47] Yi-Yan N, Felder RM, Koros WJ. Selective permeation of hydrocarbon gases in poly (tetrafluoroethylene) and poly(fluoroethylene–propylene) copolymer. J Appl Polym Sci 1980;25(8):1755–74.
[48] George SC, Thomas S. Transport phenomena through polymeric systems. Prog Polym Sci 2001;26(6):985–1017.
[49] Gårdebjer S, et al. The impact of interfaces in laminated packaging on transport of carboxylic acids. J Membr Sci 2016;518:305–12.
[50] Hjärtstam J, Hjertberg T. Effect of hydroxyl group content in ethyl cellulose on permeability in free films and coated membranes. J Appl Polym Sci 1999;72(4):529–35.
[51] Caccavo C, et al. Mathematical modeling of the drug release from an ensemble of coated pellet. Br J Pharmacol 2017;174:1797–809.
[52] Kazlauske J, et al. Determination of the release mechanism of theophylline from pellets coated with Surelease - a water dispersion of ethyl cellulose. Int J Pharm 2017;528:345–52.
[53] Kazlauske J, et al. The importance of the molecular weight of ethyl cellulose on the properties of aqueous-based controlled release coatings. Int J Pharm 2017;519:157–64.
[54] Bergstrand A, et al. Permeability of porous poly(3-hydroxybutyrate) barriers of single and bilayer type for implant applications. Int J Polym Sci 2014;2014:8.
[55] Gårdebjer S, et al. Controlling water permeability of composite films of polylactide acid, cellulose, and xyloglucan. J Appl Polym Sci 2015;132(1) (p. n/a-n/a).
[56] Gårdebjer S, et al. Using Hansen solubility parameters to predict the dispersion of nano-particles in polymeric films. Polym Chem 2016;7(9):1756–64.
[57] Rongthong T, et al. Quaternary polymethacrylate–magnesium aluminum silicate films: water uptake kinetics and film permeability. Int J Pharm 2015;490(1–2):165–72.
[58] Krasnou I, et al. Permeability of water and oleic acid in composite films of phase separated polypropylene and cellulose stearate blends. Carbohydr Polym 2016;152:450–8.
[59] Andersson H, et al. Effects of molecular weight on permeability and microstructure of mixed ethyl-hydroxypropyl-cellulose films. Eur J Pharm Sci 2013;48(1–2):240–8.
[60] Cuppok Y, et al. Drug release mechanisms from Kollicoat SR:Eudragit NE coated pellets. Int J Pharm 2011;409(1–2):30–7.
[61] Larsson M, et al. Swelling and mass transport properties of nanocellulose-HPMC composite films. Mater Des 2017;122:414–21.
[62] Zhang L, Xu T, Lin Z. Controlled release of ionic drug through the positively charged temperature-responsive membranes. J Membr Sci 2006;281(1–2):491–9.
[63] Larsson M, et al. Nanocomposites of polyacrylic acid nanogels and biodegradable polyhydroxybutyrate for bone regeneration and drug delivery. J Nanomater 2014;2014:9.
[64] Mohamaddoust Aliabadi S, et al. Polymeric composite membranes for temperature and pH-responsive delivery of doxorubicin hydrochloride. Nanomed J 2015;2(3):187–94.
[65] Manias E. Polymer nanocomposite technology, fundamentals of barrier. J Nat Mater 2007;6:9–11.
[66] Fujita H. Diffusion in polymer-diluent systems. Fortschr Hochpolym 1961;3:1–47.
[67] Cohen MH, Turnbull D. Molecular transport in liquids and glasses. J Chem Phys 1959;31(5):1164–9.
[68] Yasuda H, Lamaze CE, Ikenberry LD. Permeability of solutes through hydrated polymer membranes. Part I. Diffusion of sodium chloride. Makromol Chem 1968;118(1):19–35.
[69] Vrentas JS, Duda JL. Diffusion in polymer—solvent systems. I. Reexamination of the free-volume theory. J Polym Sci Polym Phys Ed 1977;15(3):403–16.
[70] Vrentas JS, Duda JL. Diffusion in polymer–solvent systems. II. A predictive theory for the dependence of diffusion coefficients on temperature, concentration, and molecular weight. J Polym Sci Polym Phys Ed 1977;15(3):417–39.
[71] Vrentas JS, Duda JL, Ling HC. Free-volume theories for self-diffusion in polymer–solvent systems. I. Conceptual differences in theories. J Polym Sci Polym Phys Ed 1985;23(2):275–88.
[72] Vrentas JS, Duda JL, Ling HC. Self-diffusion in polymer-solvent-solvent systems. J Polym Sci Polym Phys Ed 1984;22(3):459–69.
[73] Hong S-U, Benesi AJ, Duda JL. Use of solvent free-volume parameters from 13c relaxation to study polymer/solvent diffusion behavior. Polym Int 1996;39(3):243–9.
[74] Börjesson A, et al. Molecular modelling of oxygen and water permeation in polyethylene. Polymer 2013;54(12):2988–98.
[75] Stannett V. Permeability of plastic films and coated paper to gases and vapors. New York: Technical Association of the Pulp and Paper, Industry; 1962.
[76] Grüniger A, Rudolf von Rohr P. Influence of defects in SiOx thin films in their barrier properties. Thin Solid Films 2004;459(1–2):308–12.
[77] Christensen RM. Mechanics of composite materials. first ed. Wiley; 1979.
[78] Choy TC. Effective medium theory. Oxford University Press; 1999.
[79] Fortunati E, et al. Multifunctional bionanocomposite films of poly(lactic acid), cellulose nanocrystals and silver nanoparticles. Carbohydr Polym 2012;87(2):1596–605.
[80] Liu DU, et al. Characterisation of solution cast cellulose nanofibre - reinforced poly (lactic acid). Express Polym Lett 2010;4:26–31.
[81] Suryanegara L, Nakagaito AN, Yano H. The effect of crystallization of PLA on the thermal and mechanical properties of microfibrillated cellulose-reinforced PLA composites. Compos Sci Technol 2009;69(7–8):1187–92.
[82] Sanchez-Garcia MD, Gimenez E, Lagaron JM. Morphology and barrier properties of solvent cast composites of thermoplastic biopolymers and purified cellulose fibers. Carbohydr Polym 2008;71(2):235–44.
[83] Rhim J-W, et al. Preparation and characterization of chitosan-based nanocomposite films with antimicrobial activity. J Agric Food Chem 2006;54(16):5814–22.
[84] Gårdebjer, S., A. Bergstrand, and A. Larsson, A mechanistic approach to explain the relation between increased dispersion of surface modified cellulose nanocrystals and final porosity in biodegradable films. Eur Polym J, (0).
[85] Fredrickson GH, Bicerano J. Barrier properties of oriented disk composites. J Chem Phys 1999;110(4):2181–8.
[86] Ramanathan T, et al. Functionalized graphene sheets for polymer nanocomposites. Nat Nanotechnol 2008;3(6):327–31.
[87] Wakabayashi K, et al. Polymer-graphite nanocomposites: effective dispersion and major property enhancement via solid-state shear pulverization. Macromolecules 2008;41(6):1905–8.
[88] Compton OC, et al. Crumpled graphene nanosheets as highly effective barrier property enhancers. Adv Mater 2010;22(42):4759.
[89] Cussler EL, et al. Barrier membranes. J Membr Sci 1988;38(2):161–74.
[90] Nazarenko S, et al. Gas barrier of polystyrene montmorillonite clay nanocomposites: effect of mineral layer aggregation. J Polym Sci B 2007;45(13):1733–53.
[91] Greco A, Corcione CE, Maffezzoli A. Diffusion in oriented lamellar nanocomposite: numerical analysis of the effects of dispersion and intercalation. Comput Mater Sci 2017;133:45–51.
[92] Greco A, Maffezzoli A. Finite element modeling of multiscale diffusion in intercalated nanocomposites. J Nanomater 2015;2015:482698 [11 pages].
[93] Raj G, et al. Measuring adhesion forces between model polysaccharide films and PLA bead to mimic molecular interactions in flax/PLA biocomposite. J Mater Sci 2012;47:2175–81.
[94] Klemm D, et al. Introduction. Comprehensive cellulose chemistry. Wiley-VCH Verlag GmbH & Co. KGaA; 2004. p. 1–7.
[95] Favier V, Chanzy H, Cavaille JY. Polymer nanocomposites reinforced by cellulose whiskers. Macromolecules 1995;28(18):6365–7.
[96] Petersson L, Kvien I, Oksman K. Structure and thermal properties of poly(lactic acid)/cellulose whiskers nanocomposite materials. Compos Sci Technol 2007;67(11—12):2535–44.
[97] Petersson L, Oksman K. Biopolymer based nanocomposites: comparing layered silicates and microcrystalline cellulose as nanoreinforcement. Compos Sci Technol 2006;66(13):2187–96.
[98] Oksman K, Skrifvars M, Selin J-F. Natural fibers as reinforcements in poly lactic acid (PLA) composites. Compos Sci Technol 2003;63:1317–24.
[99] Bax B, Müssig J. Impact and tensile properties of PLA/Cordenka and PLA/flax composites. Compos Sci Technol 2008;68(7–8):1601–7.
[100] Espino-Pérez E, et al. Influence of chemical surface modification of cellulose nanowhiskers on thermal, mechanical, and barrier properties of poly(lactide) based bionanocomposites. Eur Polym J 2013;49(10):3144–54.
[101] Gårdebjer S, et al. Solid-state NMR to quantify surface coverage and chain length of lactic acid modified cellulose nanocrystals, used as fillers in biodegradable composites. Compos Sci Technol 2015;107:1–9.

[102] Carlmark A, Larsson E, Malmström E. Grafting of cellulose by ring-opening polymerisation – a review. Eur Polym J 2012;48(10):1646–59.
[103] Goffin A-L, et al. From interfacial ring-opening polymerization to melt processing of cellulose nanowhisker-filled polylactide-based nanocomposites. Biomacromolecules 2011;12(7):2456–65.
[104] Donkers PAJ, et al. Water permeability of pigmented waterborne coatings. Prog Org Coat 2013;76(1):60–9.
[105] Hjärtstam J, Hjertberg T. Studies of the water permeability and mechanical properties of a film made of an ethyl cellulose–ethanol–water ternary mixture. J Appl Polym Sci 1999;74(8):2056–62.
[106] Broadbent S, Hammersley J. Percolation processes: I. Crystals and mazes. Math Proc Camb Philos Soc 1957;53(3):629–41.
[107] Heiba AA, et al. Percolation theory of two-phase relative permability. 57th Annual fall meeting of the Society of Petroleum Engineers; 1982 [New Orleans, LA].
[108] Hammersley JM. Percolation processes - lower bounds for the critical probability. Ann Math Stat 1957;28(3):790–5.
[109] Shante VKS, Kirkpatrick S. Introduction to percolation theory. Adv Phys 1971;20 (85):325.
[110] Hunt A, et al. In: 3rd edition, editor. Percolation theory for flow in porous media. Heidelberg: Springer; 2014.
[111] Lindstedt B, Ragnarsson G, Hjärtstam J. Osmotic pumping as a release mechanism for membrane-coated drug formulations. Int J Pharm 1989;56(3):261–8.
[112] Marucci M, et al. Coated formulations: new insights into the release mechanism and changes in the film properties with a novel release cell. J Control Release 2009;136(3):206–12.
[113] Andersson H. Structure control by phase separation and influence on mass transport in films for controlled release. Department of material and manufactoring technology. Chalmers University of Technology; 2015.
[114] Marucci M, et al. Osmotic pumping release from ethyl-hydroxypropyl-cellulose-coated pellets: a new mechanistic model. J Control Release 2010;142(1):53–60.
[115] Andersson Moorea, H., et al., New insights on the influence of manufacturing conditions and molecular weight on phase-separated films intended for controlled release. Int J Pharm, [Accepted for publication].
[116] Adersjö L, et al. Addition of polysaccharides influences colloidal interactions during latex film formation along with film morphology and permeability. Langmuir 2008;24(16):8923–8.
[117] Zhang K, Wu XY. Temperature and pH-responsive polymeric composite membranes for controlled delivery of proteins and peptides. Biomaterials 2004; 25(22):5281–91.
[118] Baker JP, Siegel RA. Hysteresis in the glucose permeability versus pH characteristic for a responsive hydrogel membrane. Macromol Rapid Commun 1996;17(6): 409–15.
[119] Larsson M, Stading M, Larsson A. High performance polysodium acrylate superabsorbents utilizing microfibrillated cellulose to augment gel properties. Soft Mater 2010;8(3):207–25.
[120] Larsson M, Zhou Q, Larsson A. Different types of microfibrillated cellulose as filler materials in polysodium acrylate superabsorbents. Chin J Polym Sci 2011;29: 407–13.
[121] Bhatt B, Kumar V. Regenerated cellulose capsules for controlled drug delivery: part I. Physiological characteristics of membrane formation and the influence of thermal annealing. Cellulose 2015;22(5):3237–50.
[122] Gebäck T, et al. Investigation of the effect of the tortuous pore structure on water diffusion through a polymer film using lattice Boltzmann simulations. J Phys Chem B 2015;119(16):5220–7.
[123] Wassen S, et al. Probe diffusion in phase-separated bicontinuous biopolymer gels. Soft Matter 2014;10(41):8276–87.
[124] Gebäck T, Heintz A. A lattice Boltzmann method for the advection-diffusion equation with Neumann boundary conditions. Commun Comput Phys 2014;15 (2):487–505.